

THE UNIVERSITY OF CALGARY

Complex Ray Tracing
and
Physical Modelling:
A Comparative Study.

by

Robert W. Parney

A THESIS

SUBMITTED TO THE FACULTY OF GRADUATE STUDIES
IN PARTIAL FULFILLMENT OF THE REQUIREMENTS FOR THE
DEGREE OF MASTER OF SCIENCE

DEPARTMENT OF GEOLOGY AND GEOPHYSICS

CALGARY, ALBERTA

MAY, 1989

© Robert W. Parney, 1989



National Library
of Canada

Bibliothèque nationale
du Canada

Canadian Theses Service Service des thèses canadiennes

Ottawa, Canada
K1A 0N4

The author has granted an irrevocable non-exclusive licence allowing the National Library of Canada to reproduce, loan, distribute or sell copies of his/her thesis by any means and in any form or format, making this thesis available to interested persons.

The author retains ownership of the copyright in his/her thesis. Neither the thesis nor substantial extracts from it may be printed or otherwise reproduced without his/her permission.

L'auteur a accordé une licence irrévocable et non exclusive permettant à la Bibliothèque nationale du Canada de reproduire, prêter, distribuer ou vendre des copies de sa thèse de quelque manière et sous quelque forme que ce soit pour mettre des exemplaires de cette thèse à la disposition des personnes intéressées.

L'auteur conserve la propriété du droit d'auteur qui protège sa thèse. Ni la thèse ni des extraits substantiels de celle-ci ne doivent être imprimés ou autrement reproduits sans son autorisation.

ISBN 0-315-54306-X

THE UNIVERSITY OF CALGARY
FACULTY OF GRADUATE STUDIES

The undersigned certify that they have read, and recommended to the Faculty of Graduate Studies for acceptance, a thesis entitled, "Complex Ray Tracing and Physical Modelling: A Comparative Study" submitted by Robert W. Parney in partial fulfillment of the requirements for the degree of Master of Science.

E S Krebs

Supervisor, Dr. E. S. Krebs
Department of Geology and Geophysics

R. J. Brown

Dr. R. J. Brown
Department of Geology and Geophysics

D. C. Lawton

Dr. D. C. Lawton
Department of Geology and Geophysics

H. A. Buckmaster

Dr. H. A. Buckmaster
Department of Physics

DATE: 18 May, 1989

ABSTRACT

Ray tracing can be extended into complex space by allowing parameters such as traveltime, velocity, and the ray parameter to contain an imaginary component, in order to include the effects of internal friction (absorption) on wave propagation. An existing computational program has been modified to enable comparisons between its (synthetic) output and data which were recorded in a physical modelling tank. A numerical differentiation formula, using Lagrangian polynomials, was derived so that uneven element spacing could be used to convert particle displacement amplitudes in the original program output to hydrostatic pressure amplitudes measured by the tank receivers. Transmission and reflection coefficients were extended to include liquid-solid interfaces, so that a water and plexiglass model could be used to study the case of an elastic (non-attenuating) medium overlying an anelastic (attenuating) medium. Comparison between the tank data and the synthetic data suggests that the use of complex rays is valid. The changes of amplitude with offset did not change noticeably when the effects of absorption were ignored. Comparisons between particle displacement amplitudes and pressure amplitudes

show that displacement amplitudes are insufficient to reproduce the conditions that occur within the physical modelling tank.

ACKNOWLEDGEMENTS

It would not be possible in this limited space to name all those who supported me while this work was in progress, nor is there sufficient room to fully express my gratitude for the contributions of even one of those people. That said, I would like to thank Dr. Ed Krebs for his limitless support and inspiration, and mostly for his patience with my endless questions and tangents. I would also like to thank him for suggesting the topic and for giving me access to his complex ray-tracing software. My encounters with the physical modelling system could not have been successful without the help of Dr. Scott Cheadle, Malcom Bertram and Eric Gallant, and I would especially like to thank Scott for many hours of inspirational discussion, which helped bring some theoretical arm-waving back to the real world. It is difficult to say where all our inspirations come from, and how much our work is affected by those who came before us, those working around us, and those who tried to teach us. For this reason I would like to thank all the members of the faculty, staff and student body of the Department of Geology and Geophysics, especially my graduate school classmates. I would also like to thank my family and friends for 'being there' for me, when things got out of control.

Table of Contents

FRONTISPIECE.....	i
APPROVAL PAGE.....	ii
ABSTRACT.....	iii
ACKNOWLEDGEMENTS.....	v
Table of Contents.....	vi
List of Tables.....	ix
List of Figures.....	x
Chapter 1. INTRODUCTION.....	1
Chapter 2. MATHEMATICAL MODELLING	
2.1 Elastic Wave Theory.....	4
2.2 Absorption.....	6
2.3 Anelastic Wave Theory.....	8
Chapter 3. PREVIOUS WORK	
3.1 Historical Perspective	
of Anelastic Modelling.....	11
3.2 The Attenuation Angle.....	13
3.3 Computation of Synthetic Seismograms Using	
Complex Rays.....	16
3.4 Thesis Objectives.....	20
Chapter 4. PHYSICAL MODELLING	
4.1 Introduction.....	21

4.2 Historical Perspective	
of Physical Modelling.....	21
4.3 Parameters of the Physical Modelling Tank.....	22
4.4 Materials and Assumptions.....	23
Chapter 5. RELATIONSHIP BETWEEN PRESSURE	
AND DISPLACEMENT.....	25
Chapter 6. PROGRAM MODIFICATIONS	
6.1 Simplifying Assumptions.....	28
6.2 Numerical Differentiation and the	
Newton-Raphson Method.....	29
6.3 Lagrangian Differentiation.....	36
6.4 Calculation of Stations.....	41
6.4a Delta z	41
6.4b Traveltime and Attenuation.....	43
6.4c Geometrical Spreading.....	44
6.5 Reflection and Transmission Coefficients.....	45
6.6 Conclusion.....	50
Chapter 7. PROGRAM TESTING	
7.1 Convergence of Pressure Wavelet: Zero Offset....	52
7.2 Nonzero Offset.....	53
7.3 Constant dx and dz	55
7.4 Error Minimization.....	60

Chapter 8. TANK DATA AND WAVELET MATCHING

8.1 Introduction.....	61
8.2 Tank Data.....	61
8.3 Wavelet Matching.....	66

Chapter 9. RESULTS AND DISCUSSION

9.1 Introduction.....	74
9.2 Anelastic Modelling.....	74
9.3 Comparison to Elastic Modelling.....	81
9.4 Receiver Effects.....	86

Chapter 10. CONCLUSIONS AND FUTURE WORK..... 92

REFERENCES..... 95

List of Tables

Table 1: Model Parameters.....	24
--------------------------------	----

List of Figures

Chapter 3.

3-1: Anelastic Ray Diagram.....	14
3-2: Diagram of Ray Tracing Through Multiple Horizontal Layers.....	18

Chapter 6.

6-1: Symmetry of The Wavefront With $y = 0$	30
6-2: Determining the Pressure at a Receiver Location From Values of Particle Displacement at Nearby Station Locations.....	32
6-3: Newton-Raphson Method.....	34
6-4: Possible Convergence of Rays to a Receiver Location.....	35
6-5: Components of Displacement.....	42
6-6: Reflected and Transmitted Rays For a P Wave Incident Upon a:	
a. Solid-Solid Interface.....	47
b. Liquid-Solid Interface.....	47
c. Solid-Liquid Interface.....	47

Chapter 7.

7-1: Convergence of Lagrangian Differentiation at Zero Offset.....	54
7-2: Convergence of Lagrangian Differentiation at Non-Zero Offset.....	56
7-3: Regular Program Output.....	57
7-4: Modified Program Output: Using constant dx and dz	58
7-5: The Difference Between Variable dx , dz Output and Constant dx , dz output.....	59

Chapter 8.

8-1: Schematic of Tank Geometry.....	62
8-2: Seismic Tank Data in Standard Perkin- Elmer Format.....	64
8-3: Sample of the Tank Data in Multics Format.....	65
8-4: Extracted First Arrival and Spectrum.....	67
8-5: Comparisons of the First Reflections From the Synthetic Data and the Tank Data.....	68
8-6: Phase Rotation Plot of Synthetic First Reflection.....	70
8-7: The Difference Between the Phase Rotated Synthetic Plot and the Tank Data.....	71
8-8: Refined Phase Rotation Plot of Synthetic First Reflection.....	72
8-9: The Difference Between the Refined Phase Rotation Plot and the Tank Data.....	73

Chapter 9.

9-1: Tank Data With Direct Arrivals Removed.....	75
9-2: Synthetic Data Based On Tank Parameters, Including Attenuation.....	76
9-3: The Difference Between the Synthetic Data and the Muted Tank Data.....	77
9-4: The Difference Between the Synthetic Data Without Phase Rotation of Source Wavelet and the Tank Data.....	79
9-5: Anelastic Model Amplitude Curves Using the Full Offset Range.....	82
9-6: Elastic Model Amplitude Curves Using the Full Offset Range.....	83
9-7: Synthetic Reflection Wavelet Including Anelastic Effects and Spectrum.....	85

9-8: Synthetic Reflection Wavelet Not Including Anelastic Effects and Spectrum.....	85
9-9: Synthetic Record Showing Particle Displacement Amplitudes.....	87
9-10: The Difference Between the Displacement Synthetic and the Tank Data.....	88
9-11: Particle Displacement Amplitude Curves Including Anelastic Effects.....	89

1. INTRODUCTION

In geophysics, as in all sciences, extensive use is made of models and modelling techniques. These can take many forms: conceptual models used in the explanation of physical processes; mathematical or computer-based models that reproduce measurable quantities; physical models which mimic objects found in nature; and combinations of the above. When physics is used to delineate subsurface geology, models serve in the understanding of both the medium (the geology) and the effects of the medium on wave propagation. Models are necessary because it is not possible to sample both the medium and the wavefield completely enough to accurately measure the position of every particle as a wave travels through a medium. For example, upon the extraction of a section of the Earth, its properties (velocity, density etc..) will have been modified to such an extent that although the particle geometry is known exactly, its response to an impinging wavefield has been irreversibly changed. Therefore, in any scientific inquiry, the use of models, which can only approximate, must be carefully balanced with exacting investigations that fundamentally change what is studied.

This thesis involves a comparison between two types of models used to understand seismic experiments: (1) physical, and (2) mathematical. In the first case no approximations

are made in the wavefield and the medium geometry is measured directly, but the medium itself can only approximate the complexity that exists within the earth. In the second case, approximations are made in both the medium and the wavefield, but a greater understanding of the means by which a wavefield propagates is required. By comparing the two methods it is possible to test the completeness of this understanding, and the limits of the approximations involved.

The mathematical modelling involves ray tracing in complex space for which background theory is given in chapter 2. In chapter 3, a study of previous work in anelastic modelling, notably investigations of an elastic/anelastic boundary, is followed by a statement of the thesis objectives. Physical modelling is done in a seismic modelling tank so the fourth chapter discusses previous work in this area, as well as the technical details of the tank. The bulk of the thesis describes the conversion of a complex ray-tracing program which outputs particle displacement amplitudes, into one which produces pressure amplitudes. The relationship between displacement and pressure is derived in chapter 5, and the methods by which this relationship is implemented are discussed in chapter 6. Chapter 7 is dedicated to the testing of the program algorithm. In chapter 8 there is a discussion of the actual tank data, the water and plexiglass model which

was used to create an elastic/anelastic boundary, and the way in which the model and survey parameters were reproduced in the ray-tracing program. Chapter 9 compares the results of the two methods for an elastic/anelastic boundary, as well as the differences between anelastic and elastic models. Chapter 10 concludes with a summary and some discussion of future work.

2. MATHEMATICAL MODELLING

2.1 Elastic Wave Theory

The propagation of waves through a medium is described by Newton's second law of motion: *Force = Rate of Change of Momentum*. This can be expressed mathematically by

$$\sigma_{ij,j} + f_i = \rho \ddot{u}_i \quad [2.1-1]$$

where σ_{ij} ($i, j = 1, 2, 3$) are the components of the stress tensor; ",j" indicates partial differentiation with respect to x_j , the j th Cartesian coordinate; f_i is the i th Cartesian component of the body force; ρ the density; u_i the i th Cartesian component of the displacement field; and the double dot indicates the second partial derivative with respect to time. The Einstein summation convention is used, i.e. repeated indices indicate a summation from one to three. When modelling seismic experiments it is often assumed that the earth responds elastically to an impinging wavefield, i.e. there is no loss of energy due to absorption (see below). The stress-strain relationship for an elastic medium is given by

$$\sigma_{ij} = \lambda \delta_{ij} \epsilon_{kk} + 2\mu \epsilon_{ij}, \quad [2.1-2]$$

where L and μ are the Lamè parameters; $\delta_{ij} = 1$ if $i=j$ and zero otherwise; and the components of the strain tensor e_{ij} are given by

$$e_{ij} = \frac{1}{2} (u_{i,j} + u_{j,i}). \quad [2.1-3]$$

Substituting [2.1-3] and [2.1-2] into [2.1-1], and assuming that both L and μ are constants and that the body force $f_i = 0$, we obtain (after some algebraic manipulation)

$$(L + 2\mu)\nabla(\nabla \cdot \mathbf{u}) + \mu \nabla \times (\nabla \times \mathbf{u}) = \rho \ddot{\mathbf{u}} \quad [2.1-4]$$

where boldface indicates a vector quantity. \mathbf{u} can be written in terms of Helmholtz potentials

$$\mathbf{u} = \nabla \phi + \nabla \times \Psi, \quad [2.1-5]$$

and substituted into the equation of motion [2.1-1] to yield the wave equations

$$\nabla^2 \phi = \alpha^{-2} \ddot{\phi} \quad [2.1-6]$$

$$\nabla^2 \Psi = \beta^{-2} \ddot{\Psi}.$$

α and β are the P and S wave velocities given by

$$\alpha = \left[\frac{L + 2\mu}{\rho} \right]^{\frac{1}{2}}$$

[2.1-7]

$$\beta = \left[\frac{\mu}{\rho} \right]^{\frac{1}{2}},$$

and ϕ and Ψ are the potentials of the solenoidal ($\nabla \cdot \mathbf{u} = 0$) and irrotational ($\nabla \times \mathbf{u} = 0$) fields. The standard solution of [2.1-6] is given by

$$\phi = A e^{i(\mathbf{k} \cdot \mathbf{x} - \omega t)} \quad [2.1-8]$$

A, the amplitude, can be dependent on ω ; \mathbf{k} is the wavenumber and is such that $k^2 = \mathbf{k} \cdot \mathbf{k} = \omega^2 / \alpha^2$. The theory of elastic wave propagation has been developed much further (e.g. Aki and Richards 1980) but is only developed to this point for comparison with anelastic theory, following a discussion of absorption.

2.2 Absorption

By assuming that a medium behaves elastically it is implied that both the medium and the wavefield are not changed permanently by an encounter. However, in real-earth cases some of the wave energy is lost permanently due to internal friction, and a small amount of the induced

particle displacement within the medium is not recovered. This process is known as absorption, and a medium which behaves in this manner is said to be anelastic.

One of the parameters most commonly used to measure anelastic attenuation is the quality factor Q , and its inverse Q^{-1} (Toksöz and Johnston 1981). Q is a dimensionless ratio of stored energy to dissipated energy (ibid.) and if a volume of material is cycled in stress at a frequency ω , then $Q(\omega)$ can be expressed mathematically as:

$$\frac{1}{Q(\omega)} = - \frac{\Delta E}{2\pi E}, \quad [2.2-1]$$

where E is the peak strain energy stored in the volume and $-\Delta E$ is the energy dissipated in each cycle because of imperfections in the elasticity of the material. If no energy is lost then $Q^{-1} = 0$ and $Q = \infty$. If ΔE is non-zero then Q has a finite value and the medium is *dissipative* - i.e. a high Q value implies low attenuation.

Because energy losses due to geometrical spreading as well as reflection and transmission at boundaries are several orders of magnitude greater than those due to internal friction, the effects of absorption are often neglected in discussions of seismic experiments. This is unfortunate because parameters such as velocity, time and

depth are related to geometry, whereas Q is a material property of the medium itself.

2.3 Anelastic Wave Theory

Many attempts have been made to include the effects of absorption in mathematical models of wave propagation (see 3.1). Derivation of the anelastic wave equations was done by Bland (1960), and is presented here to contrast with the elastic case. For viscoelastic media, the time-dependent stress-strain relationship is given by

$$\sigma_{ij}(t) = \delta_{ij} L(t) * d\epsilon_{kk}(t) + 2\mu(t) * de_{ij}(t) \quad [2.3-1]$$

with the convolution defined by

$$f(t) * dg(t) = \int_{-\infty}^t f(t-\tau) \frac{dg(\tau)}{d\tau} d\tau. \quad [2.3-2]$$

In a manner similar to that for the elastic case (2.1) the substitution of [2.3-1] into the equation of motion [2.1-1] yields (after some work) (Krebes and Hron 1980a)

$$[L(t) + \mu(t)] * d(\nabla(\nabla \cdot u)) + \mu(t) * d(\nabla^2 u) = \rho \ddot{u}. \quad [2.3-3]$$

Taking the Fourier transform gives

$$(\Gamma + M) \nabla(\nabla \cdot \tilde{u}) + (M\nabla^2 \tilde{u}) = -\rho\omega^2 \tilde{u}, \quad [2.3-4]$$

where the tilde indicates the Fourier transform, and M and Γ are given by

$$M = M(\omega) = i\omega \int_0^{\infty} \mu(t) e^{-i\omega t} dt \quad [2.3-5]$$

$$\Gamma = \Gamma(\omega) = i\omega \int_0^{\infty} L(t) e^{-i\omega t} dt.$$

As before, \tilde{u} can be written in terms of Helmholtz potentials [2.1-5], and substituted into [2.3-4] to yield

$$\nabla^2 \phi + k_p^2 \phi = 0 \quad [2.3-6]$$

$$\nabla^2 \Psi + k_s^2 \Psi = 0$$

where $k_p = \omega/\alpha$ and $k_s = \omega/\beta$ are the complex wavenumbers, and the P and S wave velocities are given by $\alpha^2 = (\Gamma + 2M)/\rho$ and $\beta^2 = M/\rho$. Considering P waves, a solution similar to that for the elastic case is given by

$$\phi = \phi_0 e^{-ik \cdot x}. \quad [2.3-7]$$

k now contains both real and imaginary components such that

$$k = P - i A \quad [2.3-8]$$

where \mathbf{P} is the propagation vector, and \mathbf{A} is the attenuation vector. The implications of this formulation are explored in chapter 3.

3. PREVIOUS WORK

3.1 Historical Perspective of Anelastic Modelling

As noted earlier, much of the mathematical background for anelastic modelling was done by Bland (1960). Buchen (1971) examined the propagation of P and SU waves in linear viscoelastic media. He explored energy considerations as well as displacement and particle motion. This work was expanded by Borchardt (1973) to provide a "...mathematical framework for describing plane waves in elastic and linear anelastic media... ." He examined the propagation and attenuation vectors as well as energy considerations. Some errors occurred in the calculation of energy flux, because of non-uniqueness in his method, and these were reviewed by Krebs (1983a).

The reflection and refraction of SH waves was described by Borchardt (1977), and later extended to P and SU waves (Borchardt 1982). Borchardt gave an exact solution for the case of a general plane wave (homogeneous or inhomogeneous) incident upon an interface between two viscoelastic media. These exact solutions were an improvement on the low-loss approximations of Buchen (1971); however, they had the disadvantage of being so fully general as to limit the depth to which they could be studied analytically (Krebs 1983b). For this reason two special cases were studied by Krebs

(1983b), who found that if the quality factors (Q) of two layers are equal, then the equations describing the reflection and transmission of a homogeneous wave reduce to forms identical to the elastic case.

Silva (1976) extended the Haskell-Thompson matrix method to include the effects of attenuation, without using any low-loss assumptions. He used this method to create synthetic seismograms for models representing soils, the crust, and the core-mantle boundary. Synthetic seismograms have also been generated for teleseismic SH waves (Krebes and Hron 1980a) and for SH body waves (Krebes and Hron 1980b) travelling in a layered anelastic medium. Their work was later revised to include a more general formula for geometrical spreading (Krebes and Hearn 1985). Bourbiè and Gonzalez-Serrano (1983) created synthetic seismograms for liquid-solid and solid-solid anelastic interfaces. Their work, however, was limited to the use of potentials, and they neglected to describe the expressions used to model anelastic head-waves.

A different approach to computing synthetic seismograms was taken by Hearn and Krebes (1988). They made use of ray tracing in complex space, a method first used in EM theory (see Budden et al. 1971, Bertoni et al. 1971, Bennett 1974, Connor and Felsen 1974), and later expanded to seismology (Felsen 1984). Hearn and Krebes also used Fermat's principle to determine the initial angle between the

propagation and attenuation vectors. This removed the arbitrariness that had confronted previous authors (see below), and is the starting point for this work.

3.2 The Attenuation Angle

As was shown in (2.3), for a wave propagating through an anelastic medium the wavevector \mathbf{k} is composed of a propagation vector \mathbf{P} and an attenuation vector \mathbf{A} , such that $\mathbf{k} = \mathbf{P} - i\mathbf{A}$, with Γ defined as the angle between \mathbf{P} and \mathbf{A} (fig. 3-1). The plane wave is called homogeneous or inhomogeneous depending on whether Γ is zero or non-zero, respectively. In many calculations of synthetic seismograms for attenuating media (e.g. Krebs and Hron 1980a, Bourbiè and Gonzalez-Serrano 1983) the initial value of Γ is not known and must be arbitrarily chosen. This implies that, unlike the elastic case, raypaths in an attenuating medium are not unique (Hearn and Krebs 1988). Hearn and Krebs (1988) discussed a method, based on Fermat's principle, for determining the initial value of the attenuation angle - thus uniquely describing the raypath. Their method, using the *path of steepest descent* (see Arfken 1985 for a description of the method), produced some unexpected results for the case of a ray incident upon an elastic/anelastic boundary.

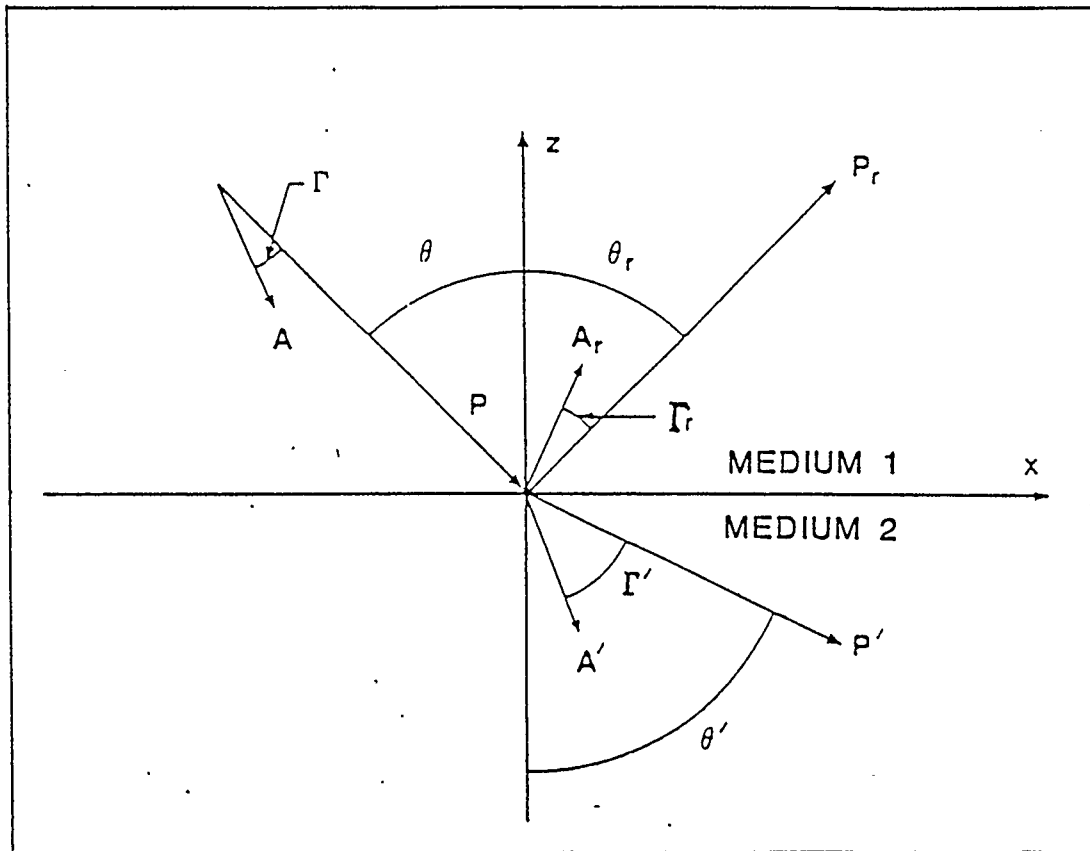


Figure 3-1: Anelastic Ray Diagram: Showing the propagation vector P , attenuation vector A , Γ the angle between them, and θ the angle of incidence for incident, reflected (subscript r) and transmitted (primed) rays.

When modelling an elastic medium using anelastic wave theory, i.e. when applying the results of the anelastic wave equations [2.3-6] to an elastic medium, the wavevector k is not attenuated (except in the case of evanescent waves). Mathematically this means that its magnitude does not contain an imaginary term. Since

$$k^2 = k \cdot k = P^2 - A^2 - 2iP \cdot A \quad [3.2-1]$$

this requires $P \cdot A = 0$, i.e.

$$P \cdot A = PA \cos \Gamma = 0. \quad [3.2-2]$$

Intuitively, this would suggest that

$$A = 0, \quad [3.2-3]$$

i.e. the magnitude of the attenuation vector is identically zero. However, equation [3.2-2] also holds if $\cos \Gamma = 0$ and $A \neq 0$, i.e.

$$\Gamma = \pm 90^\circ. \quad [3.2-4]$$

This implies that the attenuation vector may be non-zero even in the elastic case. The second possibility was found

analytically by Hearn and Krebs (1988) and confirmed computationally by Slawinski (1988).

3.3 Computation of Synthetic Seismograms Using Complex Rays

Complex ray tracing differs from standard ray tracing in that all the parameters used, such as time, velocity, reflection and transmission coefficients, and even the geometrical coordinates of a point on a ray path, are complex - i.e. contain both real and imaginary components (Hearn and Krebs 1988). Hearn and Krebs (1988) used complex ray tracing, in conjunction with the above results, to create a computer program that generated synthetic seismograms from horizontal-layer models. The program is based on an inverse Fourier transform (Krebs and Hron 1980a)

$$u = \frac{1}{\pi} \operatorname{Re} \int_0^{\infty} \frac{Y(\omega)}{L(\omega)} e^{i\phi(\omega)} S(\omega) e^{i\omega[t - \tau(\omega)]} i \, d\omega \quad [3.3-1]$$

where $Y(\omega)$ and $\phi(\omega)$ are the magnitude and phase of the product of reflection and transmission coefficients; $L(\omega)$ is the geometrical spreading; $S(\omega)$ is the spectrum of the source pulse; and u is the particle displacement at a given receiver. τ is the complex phase function such that $\tau = \tau_R + i\tau_I$, where τ_R is the arrival time of the ray and τ_I corresponds to the attenuation of the ray. i is the complex unit vector in the direction of displacement. This method has

the advantage that each frequency component can be treated separately and placed in an array, which is then transformed to the time domain by means of an inverse Fast Fourier Transform (FFT) to produce the trace.

To calculate each frequency component the complex ray parameter p must first be determined. This is given by Hearn and Krebs (1988) as:

[3.3-2]

$$p = \frac{\sin \Phi_j}{v_j} = \frac{k_x}{\omega} = \frac{P_x}{\omega} - i \frac{A_x}{\omega} = \frac{\sin \theta}{v_{IH}} - i \frac{A}{\omega} \sin(\theta - \Gamma),$$

where Φ_j is the complex incidence angle in the j th layer (fig. 3-2), and v_{IH} is the phase velocity of generally inhomogeneous waves. For a horizontally layered medium, p can be determined by numerically solving

[3.3-3]

$$X = \sum_{j=1}^m \frac{p v_j h_j}{(1 - p^2 v_j^2)^{1/2}} = \sum_{j=1}^m h_j \tan \Phi_j = \sum_{j=1}^m x_j$$

(Hearn and Krebs 1988) where h_j is the thickness associated with the j th ray segment (fig. 3-2); X is the source-receiver offset; and v_j the complex velocity. Velocity dispersion is introduced by using (Aki and Richards 1980, p. 177)

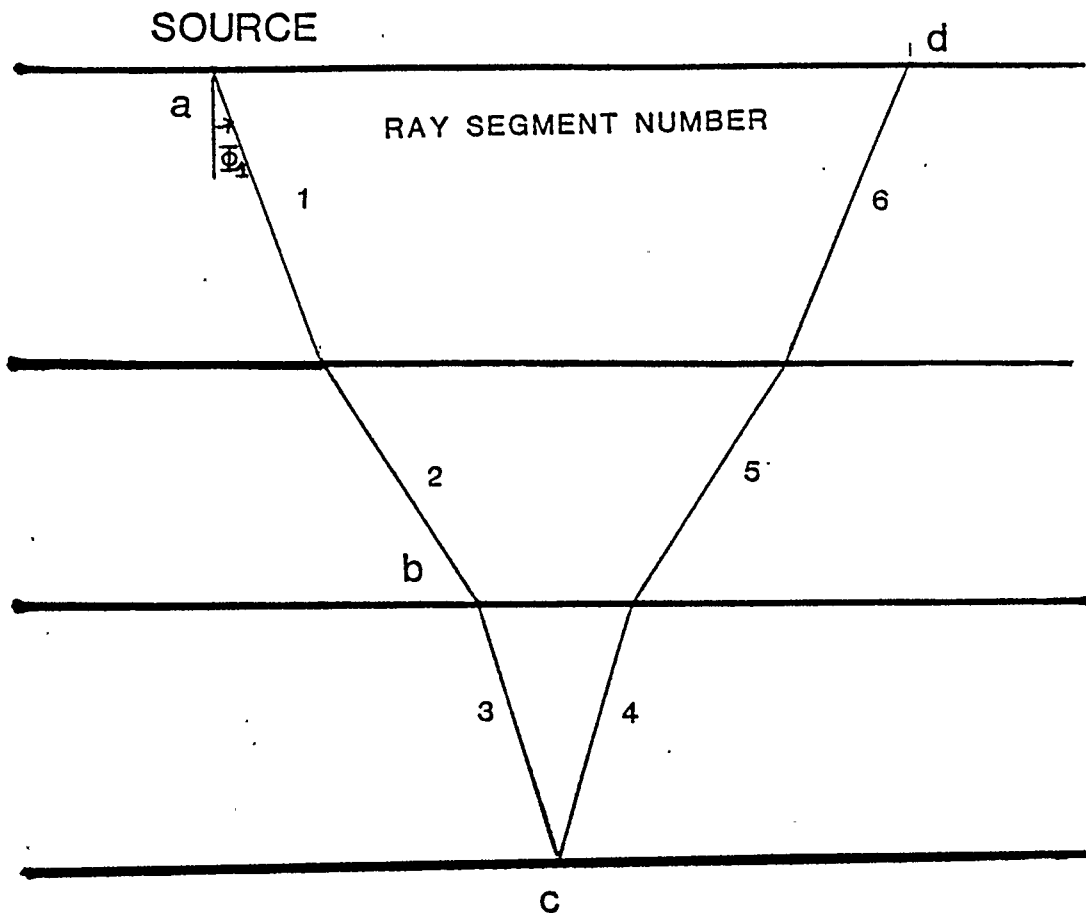


Figure 3-2: Diagram of Ray Tracing Through Multiple Horizontal Layers: 3-layer medium results in 6 ray segments, Φ_1 is the take-off angle.

$$v_H(\omega) = v_H(\omega_R) \left(1 + \frac{1}{\pi Q} \cdot \ln \frac{\omega}{\omega_R} \right), \quad [3.3-4]$$

where ω_R is the reference frequency at which Q is calculated. Once p has been determined, the traveltime can then be computed by taking the real part of τ , which is given by (Hearn and Krebs 1988):

$$\begin{aligned} \operatorname{Re}(\tau) &= \operatorname{Re} \sum_{j=1}^m \frac{h_j}{v_j \cos \Phi_j} \\ &= \operatorname{Re} \sum_{j=1}^m \frac{h_j}{v_j (1 - p^2 v_j^2)^{1/2}} \end{aligned} \quad [3.3-5]$$

Equation [3.3-3] is the result of the evaluation of the wavefield integral [3.3-1] by the method of steepest descent, for the case of a horizontally-layered anelastic medium. Note that [3.3-3] indicates that a number of complex terms must add up to give the real number X . Equation [3.3-3] is basically a system of two equations in the two unknowns θ_1 and Γ_1 . Solving the system means that θ_1 and Γ_1 , the initial values of the propagation and attenuation angles, can be uniquely determined.

Consequently, the displacement measured by a receiver, for a given survey geometry over a horizontally-layered anelastic medium, can be calculated based on input values of

layer thickness, P and S wave velocities, P and S values of Q , and rock densities.

3.4 Thesis Objectives

The object of this thesis is to modify the above mentioned program to enable complex ray tracings to be compared with laboratory data. To investigate the specific case of an elastic/anelastic boundary, data are shot in a physical modelling tank with a model composed of horizontal layers of water and plexiglass. The remaining chapters discuss physical modelling, the modification of the program used by Hearn and Krebs (1988) to output pressure amplitudes instead of displacement amplitudes, and compare the complex ray-tracing results with real data. Some comments are made about the initial choice of the attenuation angle Γ for an elastic medium.

4. PHYSICAL MODELLING

4.1 Introduction

Physical modelling can be used as an alternative to ray tracing in the examination of various aspects of seismic wave propagation. Reduced scale versions of geologic models can be made from various materials, over which seismic data can be "shot" using sources and receivers made from piezoelectric transducers (McDonald et al., 1983). The resulting seismograms are useful because no approximations are made in the wavefield, and complex geometries are as accurately tested as simple ones. The method is also ideal for testing computer models based on ray theory because, unlike field data, the "true" medium parameters can be measured directly. This chapter reviews previous work in physical modelling, and then explores the parameters of the physical modelling tank and modelling materials.

4.2 Historical Perspective of Physical Modelling

An extensive review of physical modelling up to 1983 is given by McDonald et al. (1983, p. 4), with an abridged version given here. Some of the earliest work was done by Terada and Tsuboi (1927), using agar (a type of gelatine) and an electronic chirp signal to model the effects of

faults and channels on propagation paths, as well as to examine the dispersion of Rayleigh waves. During the 1950s models made from blocks of BioPlastic™ (Evans et al. 1954), disks of metals, plastics and fibre (Oliver et al. 1954), plexiglass layers (Press et al. 1954), as well as cement and marble slabs (Levin and Hibbard 1955) were tested using piezoelectric sources and receivers. Various types of oscilloscope were used to record the output traces, with varying degrees of success. Clay and McNeil (1955) compared physical model results to elastic theory, and found they matched within reasonable limits. Silverman (1969) proposed a method of modelling involving a water tank and plexiglass models, which was the inspiration for work at the University of Houston (McDonald et al. 1983). A similar system was constructed at The University of Calgary (Cheadle et al. 1985, Cheadle 1988), from which the experimental data for this investigation were obtained.

4.3 Parameters of the Physical Modelling Tank

The modelling system at The University of Calgary consists of a water-filled tank, measuring 2 m deep by 3 m wide by 4 m long, into which models of plexiglass and other materials are placed (Cheadle 1988). The source and receiver are mounted on a system of beams and carriages which are driven by Sigma 4-V (volt) D.C. stepping motors.

International Transducer Corp. (ITC) 1089c spherical, omnidirectional hydrophones are used as both source and receivers. The source pulse is created with an initial 28-V square wave which causes the transducer to ring below its (300 kHz) resonant frequency. This is followed by a second and third square wave with variable delay time, amplitude, polarity and pulse width which are used to damp the tail oscillation (Cheadle 1988). The data are recorded through the receiving transducer and a preamplifier into an 8-bit Nicolet 2090 storage oscilloscope, at a sampling rate of 50 ns/sample. Data are then bussed through an IBM-XT to a Perkin-Elmer processing system, where (in this case) they are transferred to magnetic tape for later use on a Honeywell Multics main-frame computer. Completely automated experiments are possible since the entire system, including the source and receiver locations, is controlled by the IBM-XT.

4.4 Materials and Assumptions

In order to model the case of an elastic/anelastic boundary a simple flat layer of plexiglass is placed within the tank. The source and receiver are located in the water layer, which is assumed to act like a perfectly elastic ($Q = \infty$) medium. The plexiglass layer acts as an anelastic medium with a Q value of 50 for P waves, and a Q value of 47 for S

waves (Wuenschel 1965, Jordan 1966). A complete list of model parameters are given in table 1.

It is assumed that the transducers act as point sources and receivers. This may not be entirely valid as the ITC 1089c is composed of a piezoelectric element enclosed within

Medium	α (m/s)	β (m/s)	ρ (g/cm ³)	h (cm)	Q_p	Q_s
water	1475	-	1.00	5.8	∞	∞
plex.	2750	1375	1.19	4.2	50	47

Table 1: Model Parameters: as measured in the physical modelling tank. When anelastic effects were neglected, Q_p and Q_s were set to ∞ for the plexi-glass layer.

a 1.2 cm spherical casing, which produces a central-frequency wavelength in water of 0.63 cm (Cheadle 1988). The effect of the large receiver size is unknown but is assumed to be minimal. However, care must be taken as certain situations may occur in which the point-receiver assumption is invalid.

In most physical modelling studies, scaling assumptions are made in order to reproduce the dimension of field surveys in a laboratory setting (e.g. Hall 1956). However, no such assumptions are made here as all parameters such as velocity, distance and sample time are maintained between the computer program and the tank data.

5. RELATIONSHIP BETWEEN PRESSURE AND DISPLACEMENT

In order to compare synthetic data with tank data it is necessary to convert the ray-tracing program to output pressure amplitudes instead of displacement amplitudes. To do so it is assumed that the piezoelectric transducer which acts as a receiver measures hydrostatic pressure (see 4.4). Consequently, a fundamental relationship between hydrostatic pressure and displacement had to be established.

The equation of motion can be written

$$\rho \frac{\partial^2 u_i}{\partial t^2} = \frac{\partial \sigma_{ij}}{\partial x_j} \quad i = 1, 2, 3 \quad [5-1]$$

where ρ is the density, u_i are the components of displacement, σ_{ij} are the components of stress, and x_j are the cartesian coordinates. A fluid cannot support shear stress and normal stresses are equal in magnitude to hydrostatic pressure (Ω). Mathematically:

$$\begin{aligned} \sigma_{ij} &= 0 & i &\neq j \\ \sigma_{ij} &= -\Omega & i &= j. \end{aligned} \quad [5-2]$$

Substituting [5-2] into [5-1] we get

$$\rho \frac{\partial^2 u_i}{\partial t^2} = - \frac{\partial \Omega}{\partial x_i}, \quad [5-3]$$

where again $i = 1, 2, 3$ or

$$\rho \frac{\partial^2 u}{\partial t^2} = - (\nabla \Omega). \quad [5-4]$$

The wave equation is given by (Sheriff and Geldart 1982, p. 38):

$$(L + 2\mu)\nabla(\nabla \cdot u) - \mu \nabla \times (\nabla \times u) = \rho \frac{\partial^2 u}{\partial t^2}. \quad [5-5]$$

In the case of water, $\mu = 0$, and [5-5] becomes

$$L \nabla(\nabla \cdot u) = \rho \frac{\partial^2 u}{\partial t^2}. \quad [5-6]$$

Comparison of [5-6] with [5-4] yields

$$\Omega = -L (\nabla \cdot u), \quad [5-7]$$

for special case of a fluid. Using [5-7] we can now calculate the hydrostatic pressure numerically from the

displacement amplitudes output by the complex ray-tracing
program (chapter 3.)

6. PROGRAM MODIFICATIONS

6.1 Simplifying Assumptions

Before applying equation [5-7],

$$\Omega = -L (\nabla \cdot u),$$

its possible to make some simplifying assumptions. The data values cannot be related directly to 'true' amplitudes, because the amplitude of the tank source pulse is only measurable after significant amplification of the received signal. For this reason the program output must be scaled for comparison to tank data and the Lamè parameter L (a constant) can be omitted so that [5-7] becomes

$$\Omega = - \left[\frac{\partial u_x}{\partial x} + \frac{\partial u_y}{\partial y} + \frac{\partial u_z}{\partial z} \right], \quad [6.1-1]$$

where u_x is the x component of displacement, etc..

The middle term on the right hand side of [6.1-1] can be eliminated by symmetry arguments. The derivative of a function is defined by

$$f'(x) = \lim_{dx \rightarrow 0} \frac{f(x + dx) - f(x - dx)}{2 dx}. \quad [6.1-2]$$

A line of receivers and a source point will always lie in one particular plane. In order to compare two-dimensional ray tracing with three-dimensional physical modelling, these locations must be kept within the same vertical plane, which is defined as $y = 0$. Throughout the ray-tracing program it is assumed that energy propagates by means of plane waves. This means that in the vicinity of the receiver the wavefront is approximately straight, and the displacement vectors are all parallel to the direction of propagation. The result is that there is no y component of displacement, and the wavefront is symmetric about the plane $y = 0$ (fig. 6-1). This means that $u_y(+dy) = 0 = u_y(-dy)$, and therefore the derivative w.r.t. y , of displacement, goes to zero. Equation [6.1-1] becomes

$$\Omega = - \left[\frac{\partial u_x}{\partial x} + \frac{\partial u_z}{\partial z} \right], \quad [6.1-3]$$

and the pressure can be calculated by taking spatial derivatives of displacement.

6.2 Numerical Differentiation and the Newton-Raphson Method

In order to solve equation [6.1-3] analytically, it would be necessary to express u , given by equation [3.3-1], as a function of x and z . However, the dependence of u on z

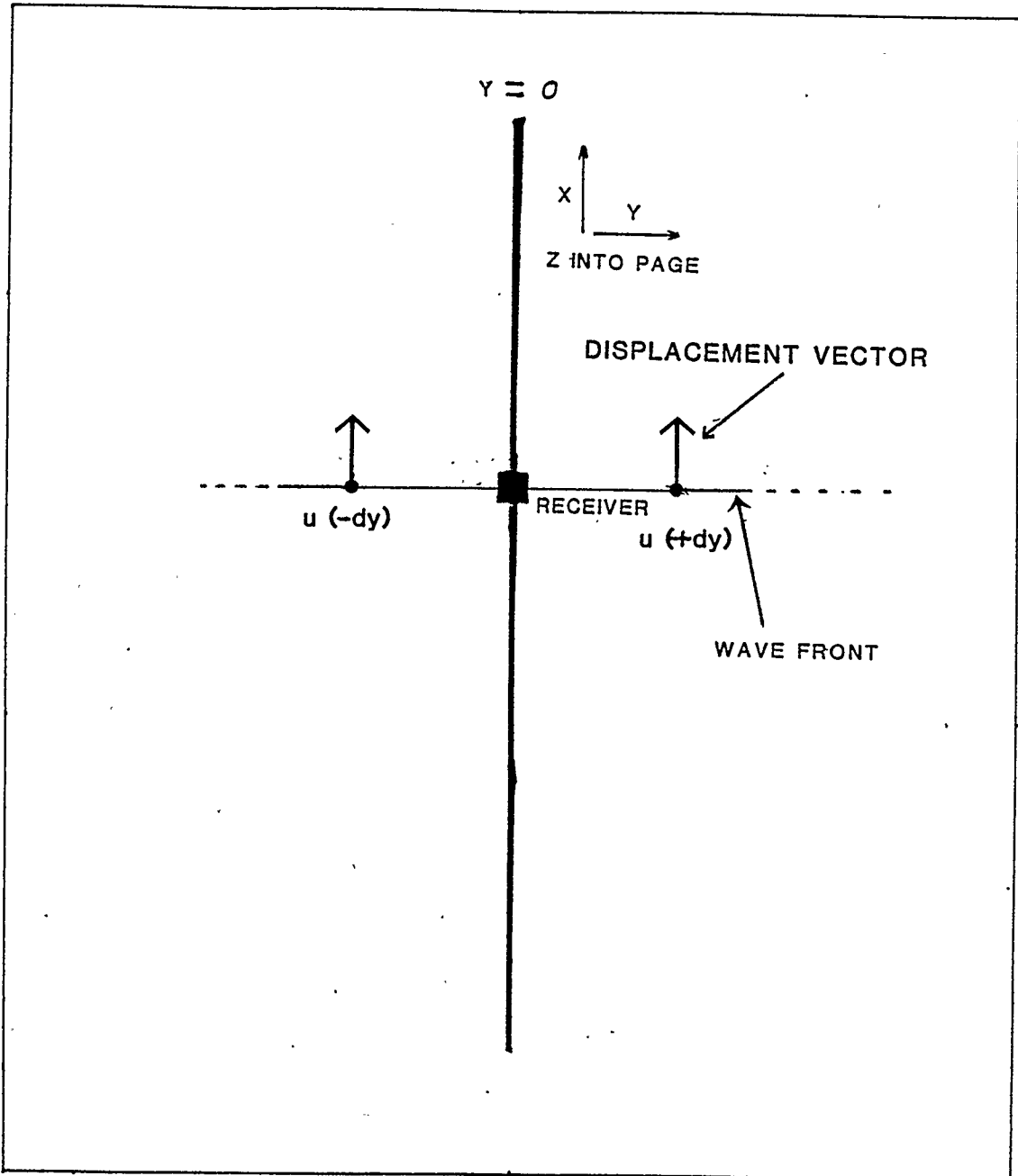


Figure 6-1: Symmetry of the Wavefront With $y = 0$: Under a plane-wave assumption $u_y(-dy) = 0 = u_y(+dy)$, i.e there is no y component of displacement and therefore $\partial u_y / \partial y \approx 0$.

can not be determined from the equations which define the components of [3.3-1] (given below), as these equations are only valid for receivers located along the line $z = 0$. Furthermore, u is only indirectly dependent on x , via the ray parameter p - i.e. x can be expressed as a function of p , using the equation for the source-receiver offset (X) over a horizontally-layered medium

$$X = \sum_{j=1}^m \frac{p v_j h_j}{(1 - p^2 v_j^2)^{1/2}}, \quad [6.2-1]$$

but it is not possible to express p (and therefor u) as a function of x . For these reasons, [6.1-3] cannot be solved analytically, and [3.3-1] must be differentiated numerically in order to calculate the pressure.

Most numerical approaches to differentiation involve equations similar to [6.1-2], where the value of the derivative of a function at a certain point x can be calculated from values of the function at points in the vicinity of x . In this case the pressure that would be measured at a certain receiver location can be calculated from the values of displacement, that would be measured at nearby stations (fig. 6-2). This involves tracing several rays in order to calculate the pressure value of a single ray. However, because of the way in which they are calculated it is possible to make use of already existing

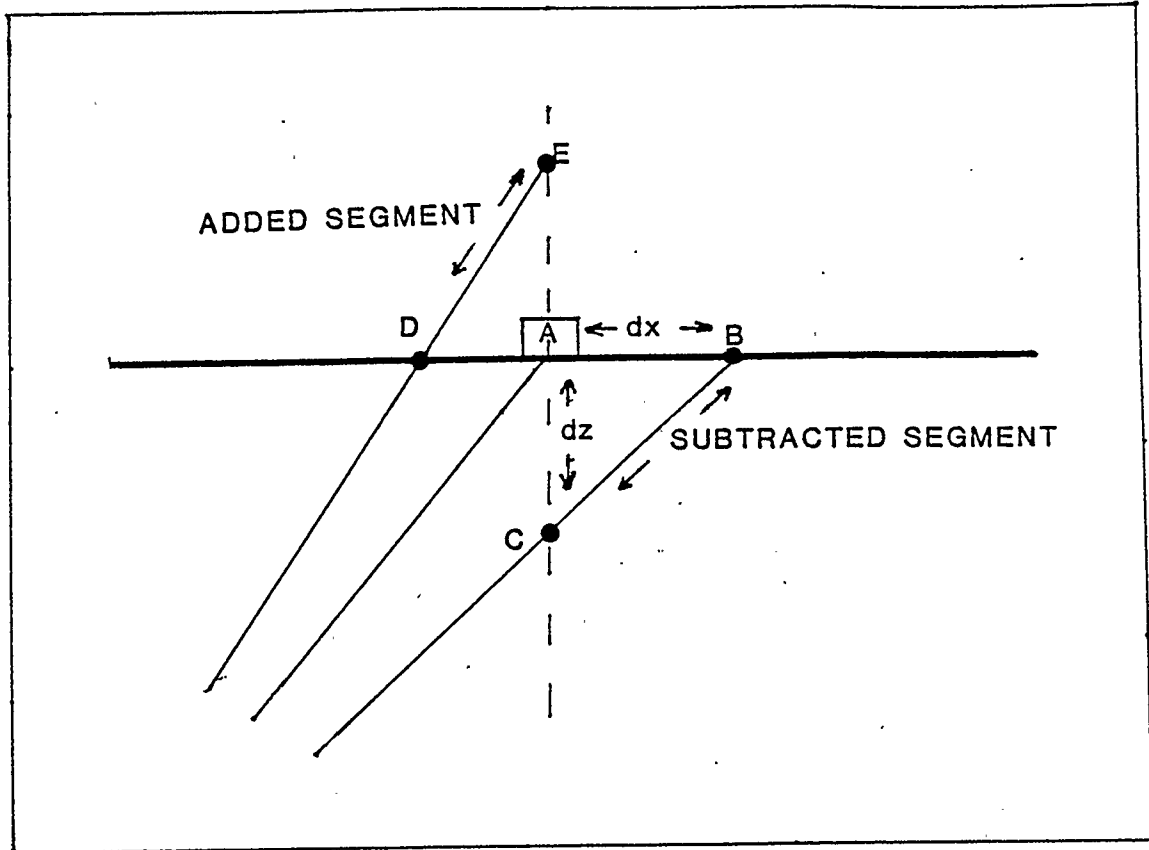


Figure 6-2: Determining the Pressure at a Receiver Location From Values of Particle Displacement at Nearby Stations: The partial derivative of u_x w.r.t. x is found from the values of u_x at stations D, A, and B using, equation [6.3-10]. The partial derivative of u_z w.r.t. z is found from the values of u_z at stations E, A, and C, and these two spatial derivatives are related to pressure by [6.1-3]. The values of u_z at stations C and E are calculated by subtracting or adding ray segments (see text) from rays which emerge at B and D respectively.

rays, and thereby reduce the additional computation time required.

In order to trace each ray, the ray parameter p must be determined for a given source-receiver offset (X), by solving [6.2-1] numerically (Hearn and Krebs 1988). This is accomplished using the Newton-Raphson method, which works as follows (Grove 1966, p. 9). If we want to solve an equation of the form $F(x) = 0$, we make a first guess x_0 and then 'draw' a tangent to the curve at the point $(x_0, F(x_0))$ (fig. 6-3). The x intercept of this line should be closer to the correct value of x , so it is used as the next approximation and the process is repeated until the solution is sufficiently accurate. Analytically, this is expressed by

$$x_{n+1} = x_n - \frac{F(x_n)}{F'(x_n)}, \quad [6.2-2]$$

so that each successive iteration is determined by the previous values of the function and its derivative. The Newton-Raphson method also works for complex functions $F(x) = 0$, such as [6.2-1]. As a result of this process there are a number of 'extra' rays which emerge at various distances from the desired receiver location (fig. 6-4). Portions can be added to or subtracted from these rays to generate stations at different z -locations (fig. 6-2), and the values

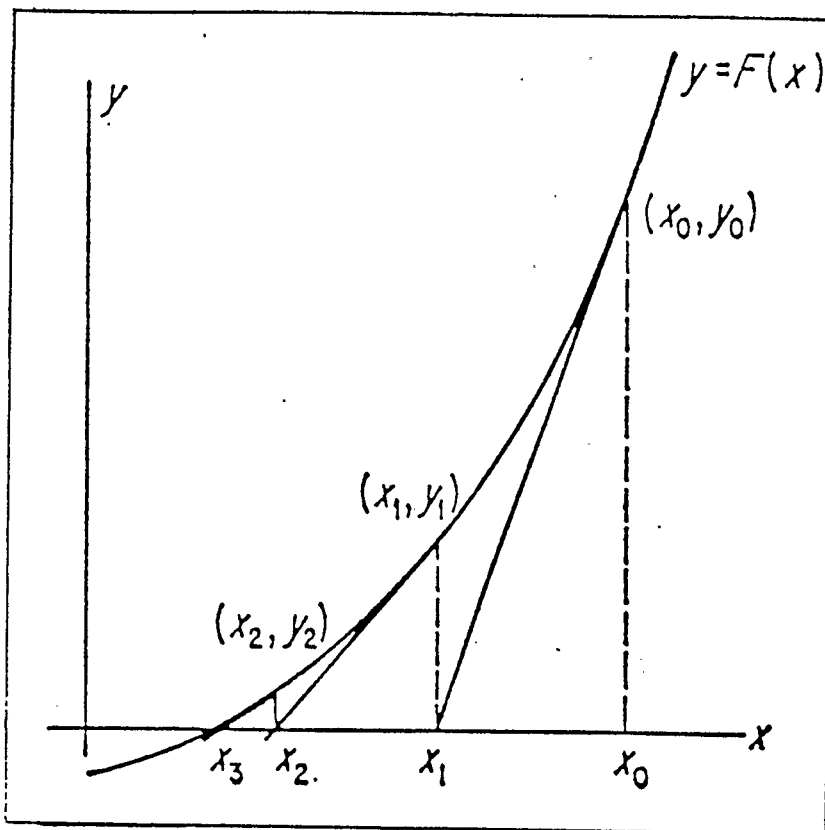


Figure 6-3: Newton-Raphson Method: x_0 is the first guess for a solution to $F(x) = 0$, x_1 is the first iteration and is found by following the derivative of $F(x)$ from (x_0, y_0) to $x = 0$.

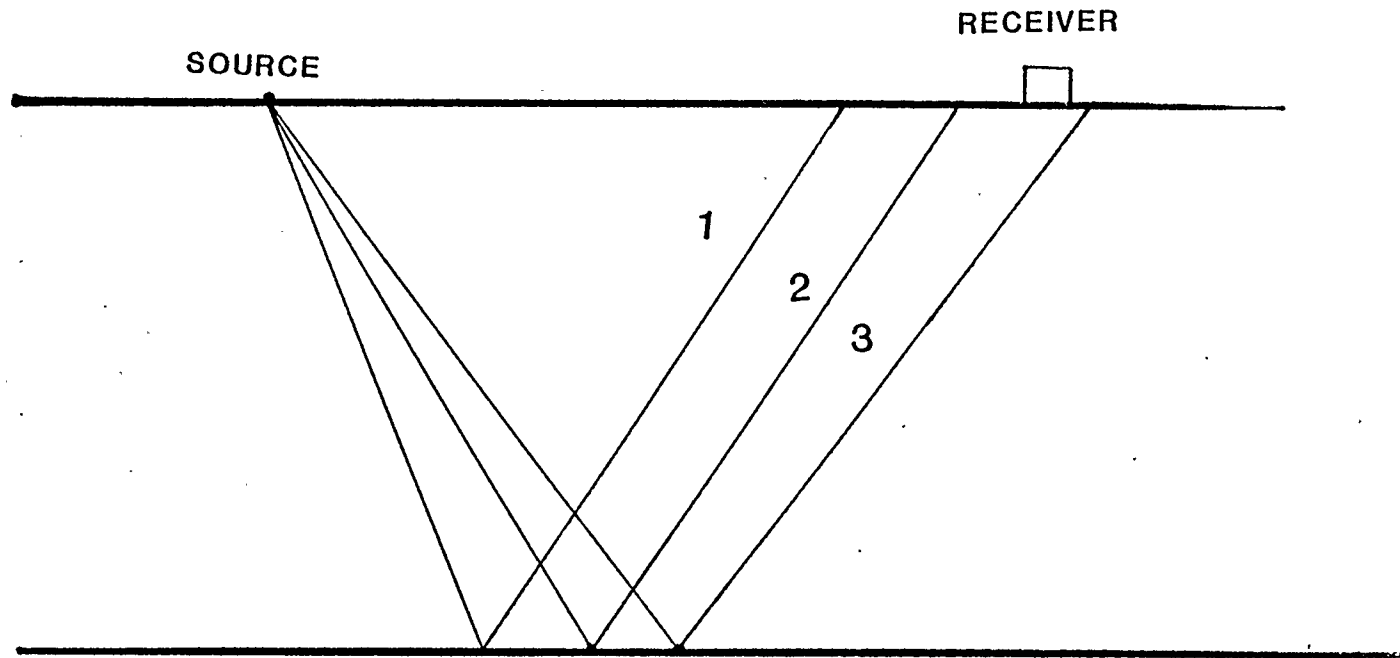


Figure 6-4: Possible Convergence of Rays to a Receiver Location: Each ray emerges closer to the receiver than the previous one, but the distance between the emergence locations may not be equal.

of displacement at these stations can then be used to calculate the pressure.

6.3 Lagrangian Differentiation

The spacing of the receiver locations due to the extra rays is somewhat irregular because the convergence rate of [6.2-2] may or may not be the same from receiver to receiver, and because the dz value (fig. 6-2) depends on both the dx value and the ray parameter (see below). Most numerical differentiation formulas require that the distance between the points at which the value of a function is known, be constant. In order to make use of the extra rays, a more general three-point formula is derived, using Lagrangian differentiation to take account of the unequal spacing. The method is similar to that used by Kelly (1967, p. 48), except that dx is not fixed.

A function $f(x)$ can be represented by

$$f(x) = \sum_{k=0}^n l_k(x) f_k + E(x), \quad [6.3-1]$$

where $l_k(x)$ is the Lagrange interpolation polynomial, $f_k \equiv f(x_k)$ where x_k are the x locations at which the value of the function is known, and $E(x)$ is the error term given by

$$E(x) = \pi(x) \frac{f^{(n+1)}(\epsilon)}{(n+1)!}, \quad [6.3-2]$$

$f^{(n+1)}$ is the $(n+1)$ st derivative of $f(x)$, ϵ is such that $x_0 \leq \epsilon \leq x_n$, $\pi(x)$ is given by

$$\pi(x) = (x - x_0)(x - x_1)(x - x_2) \dots (x - x_n), \quad [6.3-3]$$

and $l_k(x)$ is given by

$$l_k(x) = \frac{(x - x_0)(x - x_1) \dots (x - x_{k-1})(x - x_{k+1}) \dots (x - x_n)}{(x_k - x_0)(x_k - x_1) \dots (x_k - x_{k-1})(x_k - x_{k+1}) \dots (x_k - x_n)}, \quad [6.3-4]$$

If [6.3-1] is differentiated once, and the limit is set to three points ($n=2$), then

$$f'(x) \approx l_0(x) f_0 + l_1(x) f_1 + l_2(x) f_2, \quad [6.3-5]$$

with the error given by

$$E'(x) = \frac{\pi'(x) f''''(\epsilon)}{6}, \quad [6.3-6]$$

and $x_0 \leq \epsilon \leq x_2$. If [6.3-4] is limited to three points, then for the specific example of $k = 0$

$$l_0(x) = \frac{(x - x_1)(x - x_2)}{(x_0 - x_1)(x_0 - x_2)}. \quad [6.3-7]$$

Taking the derivative gives

$$l_0'(x) = \frac{(x - x_1) + (x - x_2)}{(x_0 - x_1)(x_0 - x_2)}, \quad [6.3-8]$$

or defining $dx_i \equiv x_i - x$, then $x_k - x_j = dx_k - dx_j$ and

$$l_0'(x) = \frac{-dx_1 - dx_2}{(dx_0 - dx_1)(dx_0 - dx_2)}. \quad [6.3-9]$$

If this process is repeated for $k = 1$ and 2 , and substituted into [6.3-5], the result is that

$$f'(x) = \begin{aligned} & -f_0 \left[\frac{dx_1 + dx_2}{(dx_0 - dx_1)(dx_0 - dx_2)} \right] \\ & -f_1 \left[\frac{dx_0 + dx_2}{(dx_1 - dx_0)(dx_1 - dx_2)} \right] \\ & -f_2 \left[\frac{dx_1 + dx_0}{(dx_2 - dx_1)(dx_2 - dx_0)} \right] \end{aligned} \quad [6.3-10]$$

If $\pi(x)$ is limited to three terms, i.e.

$$\pi(x) = (x - x_0)(x - x_1)(x - x_2), \quad [6.3-11]$$

then its derivative is

$$\begin{aligned} \pi'(x) &= (x - x_1)(x - x_2) + (x - x_0)(x - x_2) + (x - x_0)(x - x_1) \\ &= dx_1 dx_2 + dx_0 dx_2 + dx_0 dx_1. \end{aligned} \quad [6.3-12]$$

Substituting [6.3-12] into [6.3-6] gives the error term

$$E = \frac{[dx_1 dx_2 + dx_0 dx_2 + dx_0 dx_1] f'''(\epsilon)}{6}, \quad [6.3-13]$$

where $f(\epsilon)'''$ is the third derivative and $x_0 \leq \epsilon \leq x_2$. It is now possible to evaluate each partial derivative in [6.1-3] separately with [6.3-10].

It can be seen from [6.3-13] that the error can be minimized if the stations are chosen as close as possible to the receiver location, and on opposite sides, so that the terms within [...] tend to cancel. [6.3-10] can be tested by examining the special case where $x = x_1$, $dx_0 = -h$, $dx_2 = +h$ and therefore $dx_1 = 0$, i.e. there is equal spacing (h)

between the points and x_1 falls on the point where the derivative is to be taken. The equation becomes

$$f'(x) = -f_0 \left[\frac{h}{(-h)(-2h)} \right] - f_1 \left[\frac{0}{(+h)(-h)} \right] - f_2 \left[\frac{-h}{(+2h)(+h)} \right]$$

[6.3-14]

$$= \frac{-f_0}{2h} + \frac{f_2}{2h} = \frac{f_2 - f_0}{2h}$$

If $h = dx$, then

$$f'(x) = \frac{f(x + dx) - f(x - dx)}{2 dx} \quad [6.3-15]$$

If the limit as $dx \implies 0$ is taken, then the error term [6.3-13] drops to zero and [6.3-15] is identical to [6.1-2].

This confirms the validity of [6.3-10] for this special case, and implies that the pressure at a certain receiver location can be calculated after the values of displacement are known at nearby stations.

6.4 Calculation of Stations

Calculating the x component of the displacement at the three stations with varying x locations is a straightforward matter of multiplying the regular program output by the sine of the angle of incidence (fig. 6-5). The stations at varying z locations are created by extending or reducing rays (below) until they lie directly above or below the desired receiver location (fig. 6-2). The advantage of this method is that the ray parameter p is already known and dz can then be directly calculated (below). The reverse process is extremely difficult because the ray path is not symmetric, and p can no longer be determined by [6.2-1]. Mathematically, the extension or reduction of the rays is accomplished by changing the values of the travel-time and geometrical spreading to match the change in ray path length.

6.4a: Delta z

The first step is to calculate the distance (dz) between the station and the actual receiver location (fig. 6-2). Examination of figure (6-2) shows that, for a ray which emerges at B, the point which lies directly below the receiver A is C, and dz is given by

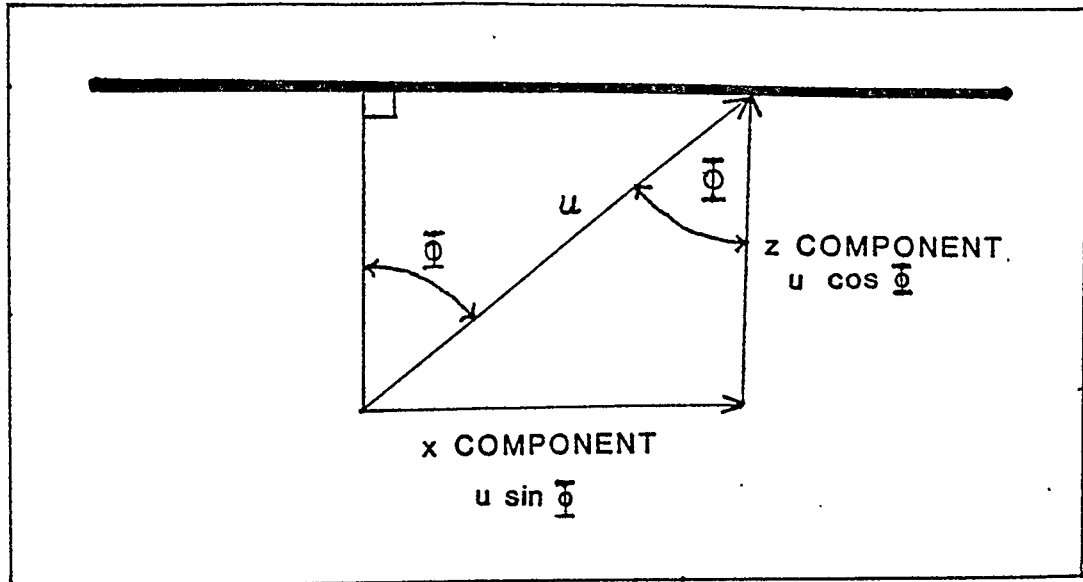


Figure 6-5: Components of displacement, and the angle (ϕ) at which the ray is incident upon the receiver.

$$dz = \frac{dx}{\tan \Phi_B}, \quad [6.4-1]$$

where Φ_B is the incidence angle of the ray, and for a horizontally layered medium is given by

$$\tan \Phi_B = \frac{\sin \Phi_B}{\cos \Phi_B} = \frac{p v_1}{(1 - (p v_1)^2)^{1/2}}. \quad [6.4-2]$$

p is the ray parameter and v_1 is the complex velocity of the first layer. Combining [6.4-1] and [6.4-2] yields

$$dz = \frac{dx (1 - (p v_1)^2)^{1/2}}{p v_1}. \quad [6.4-3]$$

Note that since p is a complex quantity, dz is a complex quantity.

6.4b: Traveltime and Attenuation

The phase function τ is given by

$$\tau = \sum_{j=1}^m (\Delta_j / v_j) \quad [6.4-4]$$

(Hearn and Krebs 1988), where s_j is the complex arc length. The traveltime of the ray is $\text{Re}(\tau)$ and the $\text{Im}(\tau)$ is related to attenuation. The traveltime and attenuation from B to C (fig. 6-2) must be corrected by removing the effects of arc length BC on τ , after the calculation of dz . If τ_B is defined as the phase function calculated at point B, then the corrected phase function at point C is given by

$$\tau_C = \tau_B - \left[\frac{(dx^2 + dz^2)^{1/2}}{v_1} \right]. \quad [6.4-5]$$

For station E (fig. 6-2) a similar process is invoked, except that the component in the square brackets is added instead of subtracted.

6.4c: Geometrical Spreading

The formula for geometrical spreading in the elastic case is given by

$$L_e = \frac{\cos \theta_0}{v_0} \left[\left[\sum_{j=1}^m \frac{v_j h_j}{\cos \theta_j} \right] \left[\sum_{j=1}^m \frac{v_j h_j}{\cos^3 \theta_j} \right] \right]^{1/2}, \quad [6.4-6]$$

(Krebes and Hearn 1985) where θ_j is the angle that the j th ray segment makes with vertical; v_j is the velocity associated with a the j th ray segment; and h_j is the thickness associated with the j th ray segment (fig. 3-2). Hearn and Krebes (1988) suggest that equation [6.4-6] can be extended into complex space by allowing all the parameters to become complex, and that it thus remains valid for anelastic media. Since the summations are taken over the number of ray segments, not the number of layers (fig. 3-2), correcting to the stations above and below the receiver becomes a simple matter of adjusting the thickness of the layer in which the last ray travels.

6.5 Reflection and Transmission Coefficients

The reflection and transmission coefficients used in the program were derived from the *Zoeppritz equations* [6.5-1,4], which express the boundary conditions for a ray impinging upon an interface between two solids (fig. 6-6a). The following quantities are continuous across the boundary:

1. The x component of displacement (u_x),

[6.5-1]

$$(P_I + P_R) \sin \theta_1 + (S_I + S_R) \cos \theta_1 = P_T \sin \theta_2 + S_T \cos \theta_2;$$

2. The z component of displacement (u_z),

[6.5-2]

$$(P_I - P_R) \cos \theta_1 - (S_I - S_R) \sin \theta_1 = P_T \cos \theta_2 - S_T \sin \theta_2;$$

3. Shear stress (σ_{xz}),

$$2\rho_1\beta_1^2 p(P_I - P_R) \cos \theta_1 + \rho_1\beta_1(1 - 2\beta_1^2 p^2)(S_I - S_R) =$$

$$2\rho_2\beta_2^2 pP_T \cos \theta_2 + \rho_2\beta_2(1 - 2\beta_2^2 p^2) S_T;$$

[6.5-3]

4. Normal stress (σ_{zz}),

$$\rho_1\alpha_1(1 - 2\beta_1^2 p^2)(P_I + P_R) - 2\rho_1\beta_1^2 p(S_I + S_R) \cos \theta_1 =$$

$$\rho_2\alpha_2(1 - 2\beta_2^2 p^2) P_T - 2\rho_2\beta_2^2 pS_T \cos \theta_2.$$

[6.5-4]

In these equations P and S are the P and S wave amplitudes; the subscripts I , R , and T refer to the incident, reflected, and transmitted waves; θ and θ refer to the angles that the P and S rays make with against vertical; and subscripts 1 and 2 indicate incident or transmitted angle. The reflection and transmission coefficients derived from these equations are given by Aki and Richards (1980, p. 150). However, if one of the media does not support S waves, as with the case of the water layer in the tank model, then [6.5-1] is invalid and the reflection and

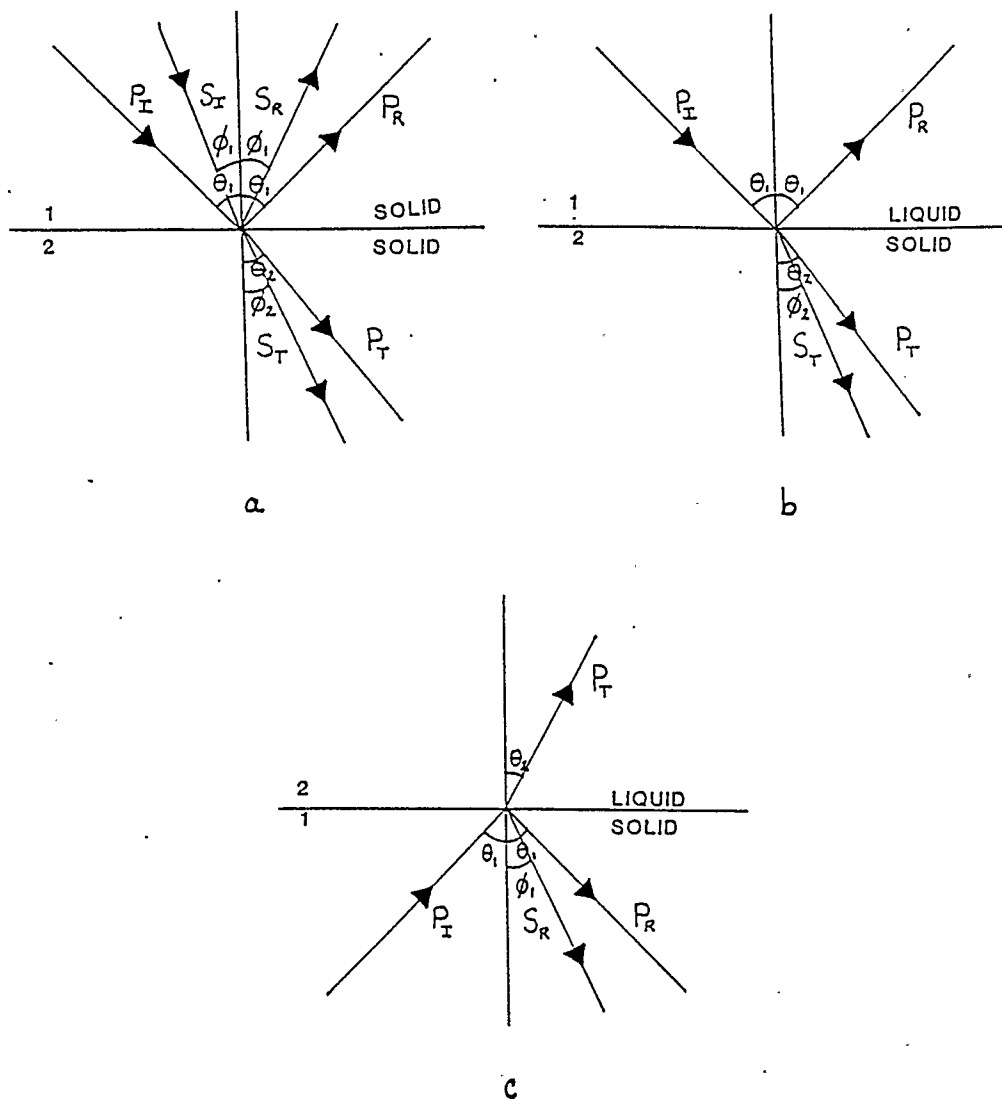


Figure 6-6: Reflected and Transmitted Rays for a P Wave Incident Upon a: a) Solid-solid interface; b) Liquid-solid, P incident from liquid layer; c) Solid-liquid, P incident from solid layer.

transmission coefficients must be derived from somewhat different boundary conditions.

Assuming a P wave incident from an overlying water layer onto a liquid-solid interface (fig. 6-6b), then $\beta_1 = 0$ and $S_I = S_R = 0$. If $P_I \equiv 1$, then P_T is the transmission coefficient etc..., and the boundary conditions [6.5-2 to 4] become:

$$u_z: \cos \theta_1 (P_R) + \cos \theta_2 (P_T) - \beta_2 p (S_T) = \cos \theta_1 \quad [6.5-5]$$

$$\sigma_{xz}: 2\beta_2 p \cos \theta_2 (P_T) + (1 - 2\beta_2^2 p^2) (S_T) = 0 \quad [6.5-6]$$

$$\sigma_{zz}: -\rho_1 \alpha_1 (P_R) + \rho_2 \alpha_2 (1 - 2\beta_2^2 p^2) (P_T) - 2\rho_2 \beta_2^2 p \cos \theta_2 (S_T) = \rho_1 \alpha_1. \quad [6.5-7]$$

Solving [6.5-5 to 7] leads to the following reflection and transmission coefficients for a P wave incident on a liquid-solid interface:

$$[6.5-8]$$

$$P_{inc.} - P_{refl.} = (M)^{-1} [-\rho_1 \alpha_1 \cos \theta_2 + \rho_2 \alpha_2 \cos \theta_1 (1 - 2\beta_2^2 p^2)^2 + 4 \rho_2 \beta_2^3 p^2 \cos \theta_1 \cos \theta_2 \cos \theta_2]$$

$$P_{inc.} - P_{trans.} = (M)^{-1} [2\rho_1 \alpha_1 \cos \theta_1 (1 - 2\beta_2^2 p^2)] \quad [6.5-9]$$

$$P_{inc.} - S_{trans.} = (M)^{-1} [-4\rho_1 \alpha_1 \beta_2 p \cos \theta_1 \cos \theta_2], \quad [6.5-10]$$

where

$$M \equiv \rho_1 \alpha_1 \cos \theta_2 + \rho_2 \alpha_2 \cos \theta_1 (1 - 2\beta_2^2 p^2)^2 + 4\rho_2 \beta_2^3 p^2 \cos \theta_1 \cos \theta_2 \cos \phi_2. \quad [6.5-11]$$

For the case of a P wave incident on a solid-liquid interface (fig. 6-6c), i.e. if medium 1 is the solid and medium 2 the liquid, then $P_I \equiv 1$, $S_I \equiv 0$, $\beta_2 = 0$ and $S_T = 0$. The boundary conditions [6.5-2 to 4] become:

$$u_z: \cos \theta_1 (P_R) + \cos \theta_2 (P_T) - \beta_1 p (S_R) = \cos \theta_1 \quad [6.5-12]$$

$$[6.5-13]$$

$$\sigma_{xz}: 2\beta_1 p \cos \theta_1 (P_R) + (1 - 2\beta_1^2 p^2) (S_R) = 2\beta_1 p \cos \theta_1$$

$$\sigma_{zz}: -\rho_1 \alpha_1 (1 - 2\beta_1^2 p^2) (P_R) + \rho_2 \alpha_2 (P_T) + 2\rho_1 \beta_1^2 p \cos \phi_1 (S_R) = \rho_1 \alpha_1 (1 - 2\beta_1^2 p^2). \quad [6.5-14]$$

Solving [6.5-12 to 14] yields the reflection and transmission coefficients for a P wave incident upon a solid-liquid interface:

$$[6.5-15]$$

$$P_{inc.} - P_{refl.} = (N)^{-1} [\rho_2 \alpha_2 \cos \theta_1 - \rho_1 \alpha_1 \cos \theta_2 (1 - 2\beta_1^2 p^2)^2 + 4 \rho_1 \beta_1^3 p^2 \cos \theta_2 \cos \theta_1 \cos \phi_1]$$

$$P_{inc.} - P_{trans.} = (N)^{-1} [2\rho_1\alpha_1 \cos \theta_1 (1 - 2\beta_1^2 p^2)] \quad [6.5-16]$$

$$P_{inc.} - S_{refl.} = (N)^{-1} [4\rho_1\alpha_1\beta_1 p \cos \theta_2 \cos \theta_1 \quad [6.5-17] \\ \times (1 - 2\beta_1^2 p^2)]$$

where

$$N \equiv \rho_2\alpha_2 \cos \theta_1 + \rho_1\alpha_1 \cos \theta_2 (1 - 2\beta_1^2 p^2)^2 \quad [6.5-18] \\ + 4\rho_1\beta_1^3 p^2 \cos \theta_2 \cos \theta_1 \cos \theta_1.$$

The addition of [6.5-8 to 11] and [6.5-15 to 18] to the ray-tracing program, with all the parameters except the density complex, now enables models including water layers to be examined.

6.6 Conclusion

Starting with some simplifying assumptions, a method has been proposed which converts displacement amplitudes to pressure amplitudes. A formula has been derived which allows unequal station spacing, and which reduces to a standard two point differentiation formula if the spacing remains constant. Stations are created by using rays which emerge near the receiver, with some addition or subtraction of ray segments to create stations above and below the

receiver. This method is tested numerically in the next chapter.

7. PROGRAM TESTING

7.1 Convergence of Pressure Wavelet: Zero Offset

Before comparisons can be made between the program output and the tank data two steps must be taken: 1. testing of the finite difference method, and 2. matching of the source wavelet. One way to test the method is to examine the effect on the output of changing the values of dx and dz . The simplest case to test is that of a zero-offset receiver, because at zero offset the receiver is symmetric (in x) with respect to the reflected wave fronts. The argument (6.1), used to show that

$$\frac{\partial u_y}{\partial y} = 0,$$

can now be used to show that

$$\frac{\partial u_x}{\partial x} = 0, \quad [7.1-1]$$

because of the symmetry in x . Consequently, the pressure is a function of only

$$\frac{\partial u_z}{\partial z}$$

Figure (7-1) shows the effect on the wavelet of changing dz . Each trace represents a zero-offset ray overlying a single reflector at 2 km depth, where the P -wave velocity in the first medium is 2 km/s. dz varies by an order of magnitude between traces, starting at 10 km, then 1 km, 0.1 km and so on down to 10^{-8} km. At $dz = 10$ km the result is just noise, as can be seen on trace 1. On the next two traces, $dz = 1$, 0.1, two wavelets are visible and they converge when $dz = 10^{-2}$. There are subtle changes in the wavelet between $dz = 10^{-2}$ and $dz = 10^{-3}$ (traces 4 and 5), but between $dz = 10^{-3}$ and $dz = 10^{-6}$ (traces 5 through 8) the wavelet remains constant. Some noise appears when $dz = 10^{-7}$ (trace 9) and the wavelet broadens and artifacts appear when $dz = 10^{-8}$ (trace 10). The effects on the last two traces are probably due to rounding errors that occur as the difference between $u(+dz)$ and $u(-dz)$ approaches accuracy limitations within the computer.

7.2 Nonzero Offset

The effect of varying both dx and dz can be tested by repeating the process for an offset of 2.5 km. For a single layer p can be found directly instead of numerical solution

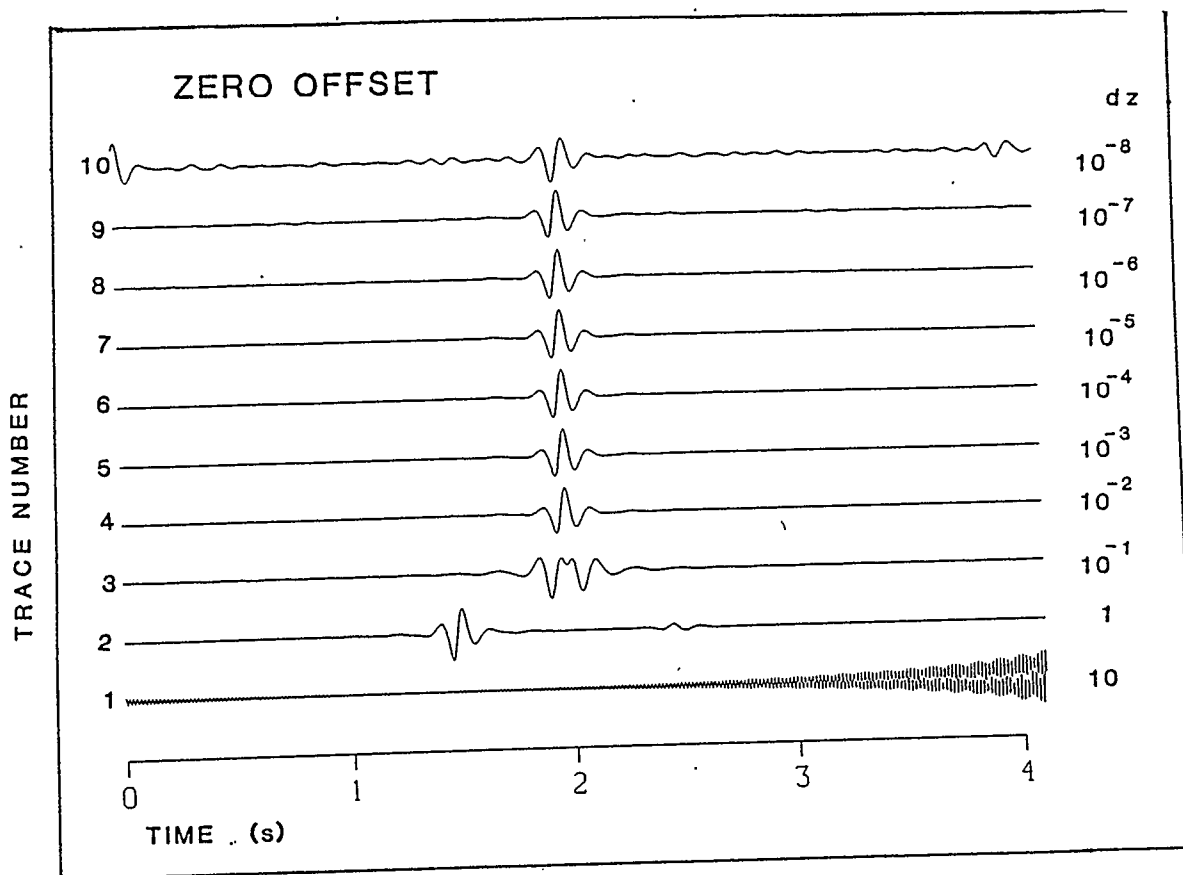


Figure 7-1: Convergence of Lagrangian Differentiation at Zero Offset: Computer plot where each trace is at the same offset but the dz value (see fig. 6-2) is changed from 10 km to 10^{-8} km. Note the wavelet remains stable between traces 5 through 8.

of [3.3-3]. dx can then be fixed and dz calculated using [6.4-3]. In figure (7-2) each trace is fixed at an offset of 2.5 km, and dx varies by an order of magnitude between traces. As before, $dx = 10$ km (trace 1) contains only noise. Between $dx = 1$ and $dx = 10^{-2}$ km (traces 2 through 4) the wavelet is converging, and between $dx = 10^{-3}$ and $dx = 10^{-6}$ (traces 5 through 8) the wavelet is stable. Noise and artifacts appear for $dx \leq 10^{-7}$ (traces 9 and 10).

7.3 Constant dx and dz

One further test was run. In this case the normal output of the program was compared to the output of a program which had been modified to keep $dx = dz = C$ (a constant value) at all stations. This is easily implemented for a single reflector but would require many extra calculations for multiple layers. The regular program output is given in figure (7-3) and the constant dx, dz output is given in figure (7-4). There is no visible difference between the two plots, as their subtraction given in figure (7-5) demonstrates. For this reason, it was concluded that any accuracy gained by keeping dx and dz constant was negated by the substantial increase in computation time required to do so.

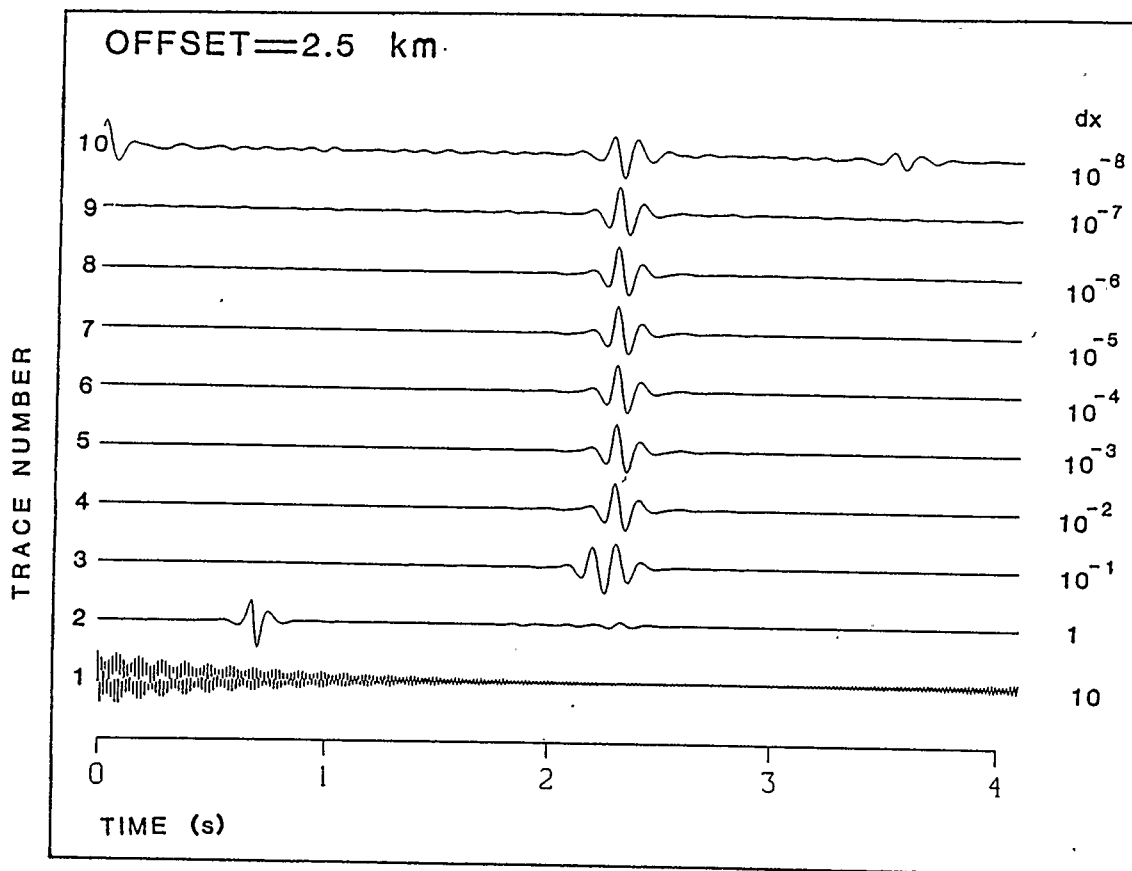


Figure 7-2: Convergence of Lagrangian Differentiation at Non-Zero Offset: Computer plot where each trace is at the same offset but the dx value (see fig. 6-2) is changed from 10 km to 10^{-8} km. The dz value is calculated from dx using equation [6.4-1]. Note the wavelet remains stable between traces 5 through 8.

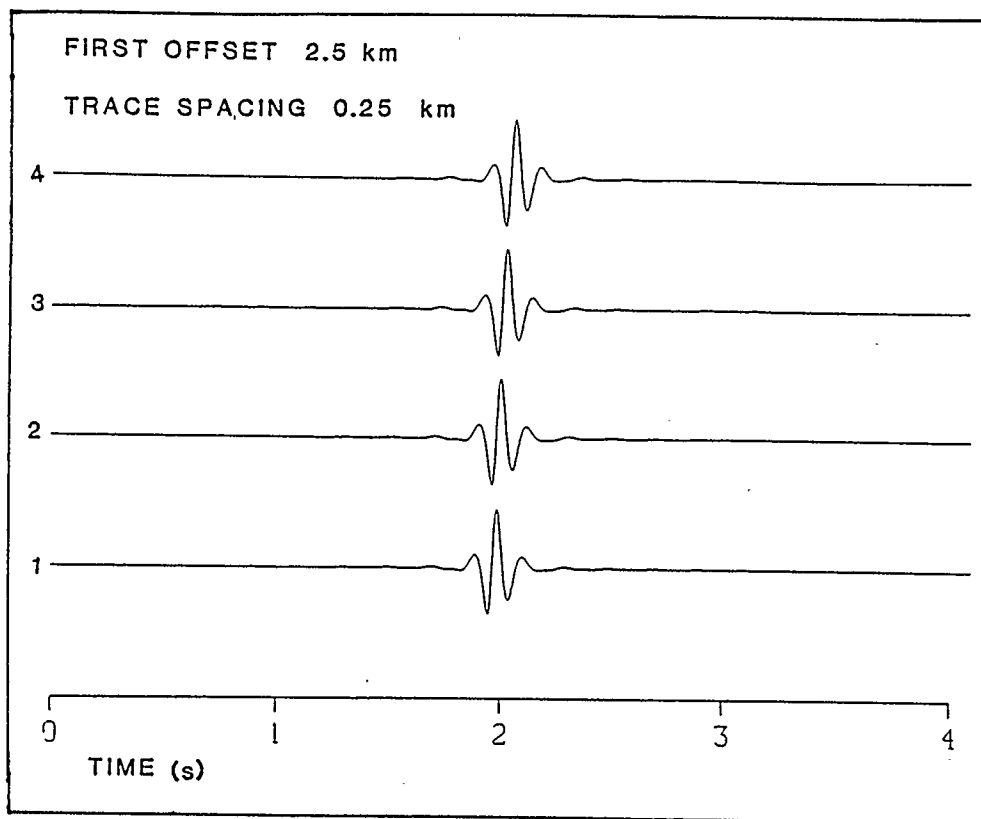


Figure 7-3: Regular Program Output: Variable dx and dz .

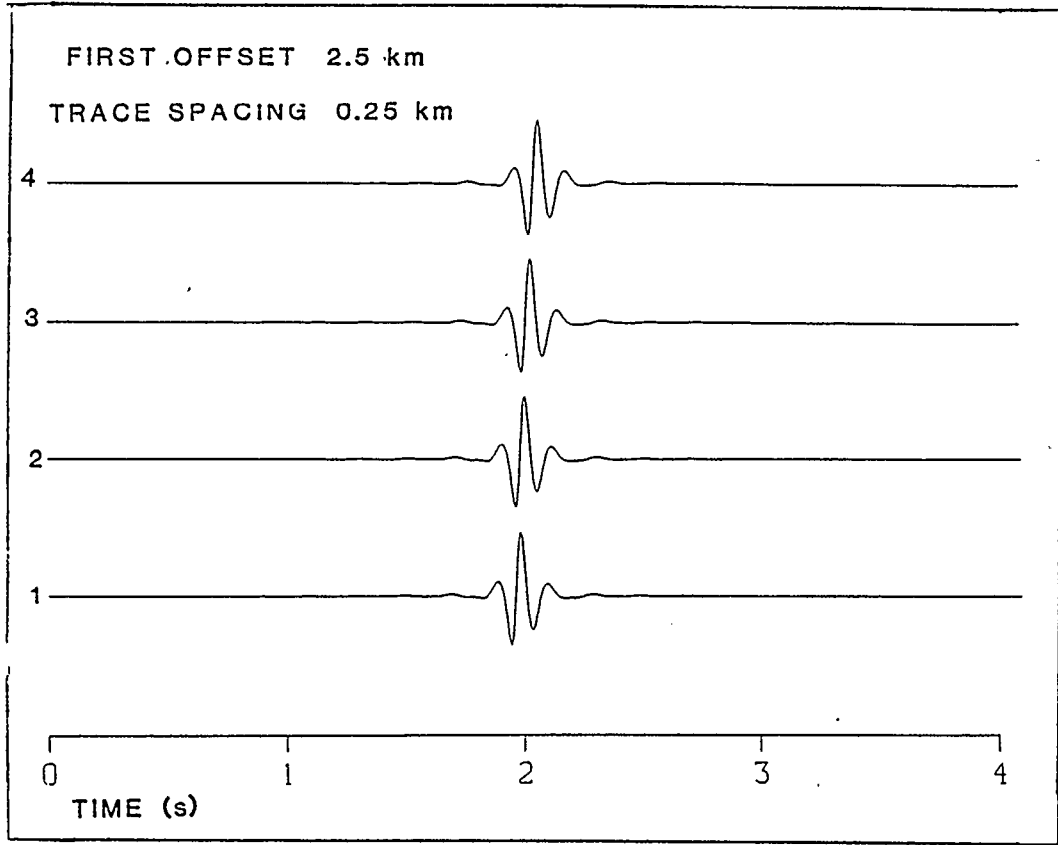


Figure 7-4: Modified Program Output: Using constant dx and dz .

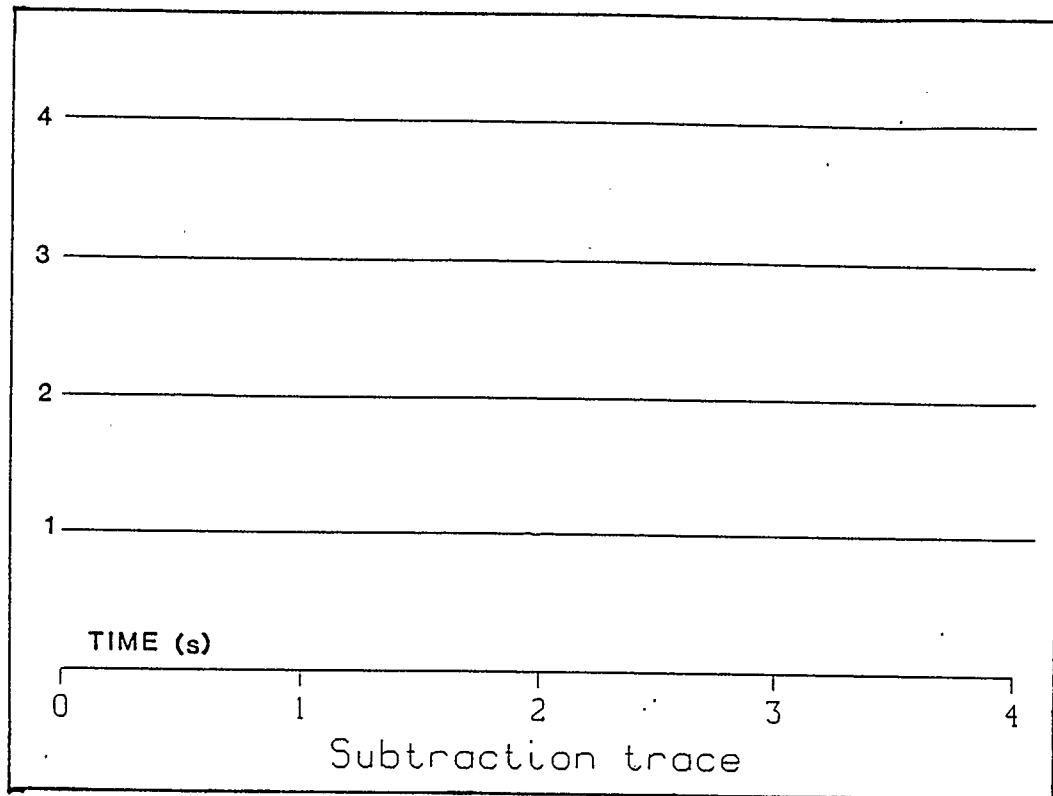


Figure 7-5: The Difference Between Variable dx , dz output (fig. 7-3) and Constant dx , dz Output (fig. 7-4): The scaling used is the same as in the previous two figures. The lack of any difference between the two outputs indicates that constant station spacing is not required.

7.4 Error Minimization

From this it was concluded that a sufficiently accurate solution would be achieved if the values of dx and dz were restricted to the 10^{-3} to 10^{-6} km range. As was noted in section (6.3) the error can be further minimized by selecting rays such that dx_0 and dx_2 have opposite signs - i.e. the station locations are on opposite sides of the receiver location. It turns out that the Newton-Raphson method tends to converge by the second iteration, so a third ray had to be added. This was done by 'shooting' a ray using a p value found by adding the difference between the first two p values to the value of p at the receiver location. The end result was that $dx_0 \approx -dx_2$, and $dx \approx 0$ - effectively minimizing the error.

8. TANK DATA AND WAVELET MATCHING

8.1 Introduction

In this chapter the connection between the data shot in the modelling tank and the synthetic data is examined. After the program had been modified to output pressure values, the model geometry and the source wavelet had to be reproduced. For this reason the tank data are examined first, as are some problems caused by the survey geometry. The process by which the source wavelet was introduced to the complex ray-tracing program is then explored.

8.2 Tank Data

The method by which the data were acquired is discussed in chapter 4. The model used in this case was a flat section of plexiglass, 4.2 cm thick, which was placed within the modelling tank, on a table made from PVC plastic (fig. 8-1). The bottom of the spherical transducer was located 5.8 cm above the plexiglass-water interface, and separated initially by 0.5 cm. The survey was then run automatically with 120 shots taken at 0.1 cm spacings. At each location, 4096 samples were taken at intervals of 50 ns, to give a total trace length of 204.8 μ s. At each receiver location this process was repeated 10 times with the results added

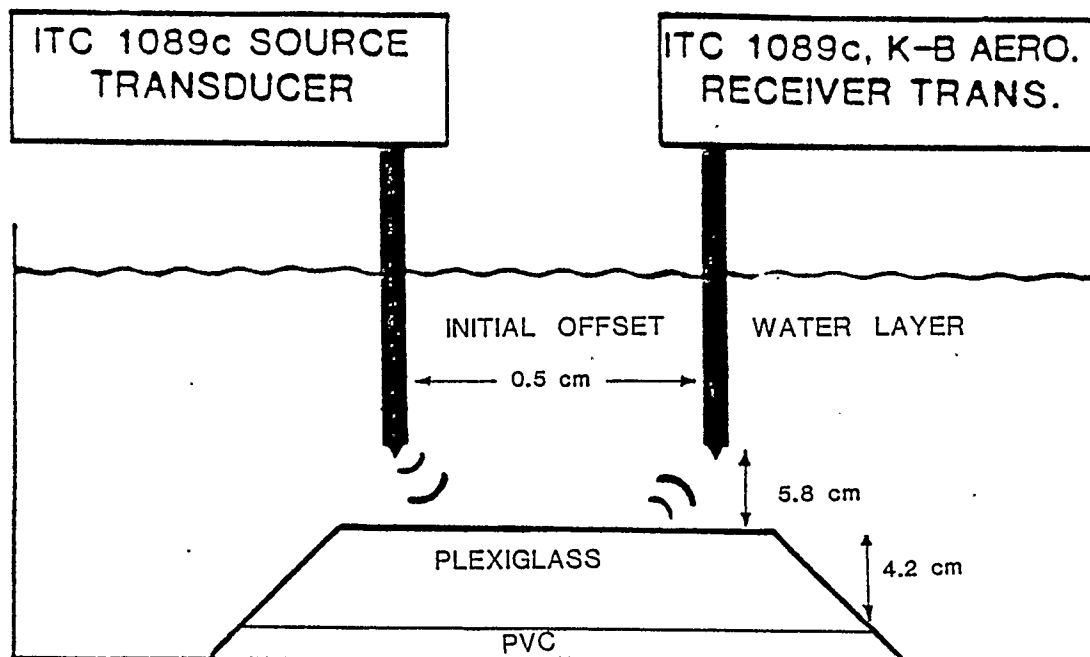


Figure 8-1: Schematic of Tank Geometry (modified from Cheadle 1988).

(stacked) together to reduce random noise - a standard procedure. A plot of the data is given in figure (8-2), with a close up in figure (8-3). Three distinct events appear: 1. The direct arrival between the source and receiver, 2. An event due to the water/plexiglass contact, and 3. An event due to the PVC/water contact below the table. The velocities and densities of PVC and plexiglass are such that there exists no impedance contrast between them (Cheadle 1988), and therefore no event occurs at the plexiglass/PVC contact.

Some time delay occurs in the transducers (Cheadle 1988), either in the electrical response, or as the wave travels through the outer shell to the piezoelectric element. This means that although the shot geometry can be measured in the tank the initial distance between the source and receiver, and the depth to the first layer, must be calculated exactly from the data. The slope of the first breaks yields a P wave velocity of 1475 m/s for water, well within the range found by Cheadle (1988). The intercept of the first breaks with the $t = 0$ axis indicates that the first source-receiver offset was 1.21 cm, somewhat larger than the 0.5 cm offset measured originally. This implies that a physical gap equivalent to 0.355 cm of water exists at each transducer, which appears reasonable given their dimensions. If this distance is added to the depth

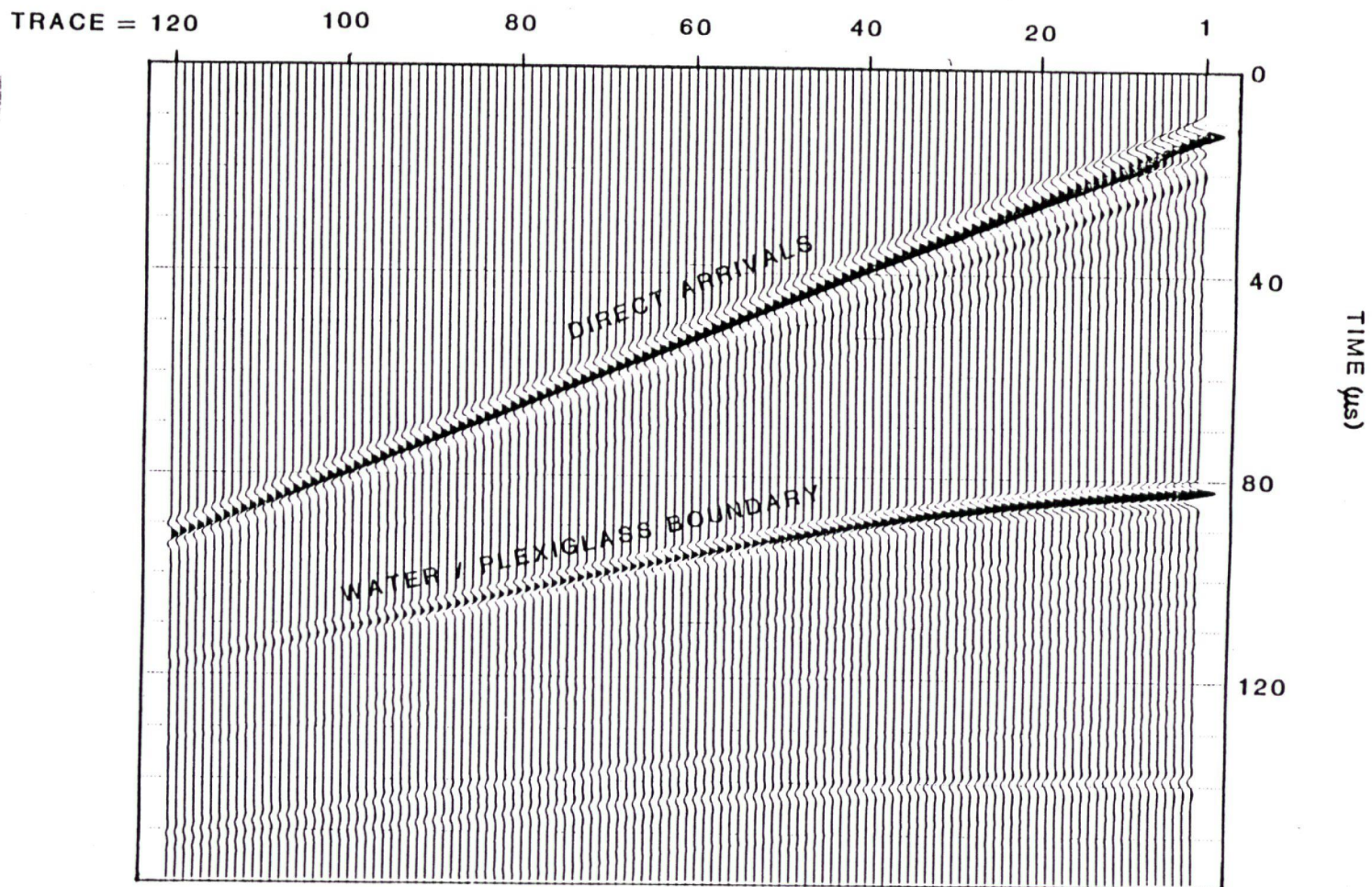


Figure 8-2: Seismic Tank Data in Standard Perkin-Elmer Format: A gain of 3×10^{-2} was applied to all the traces.

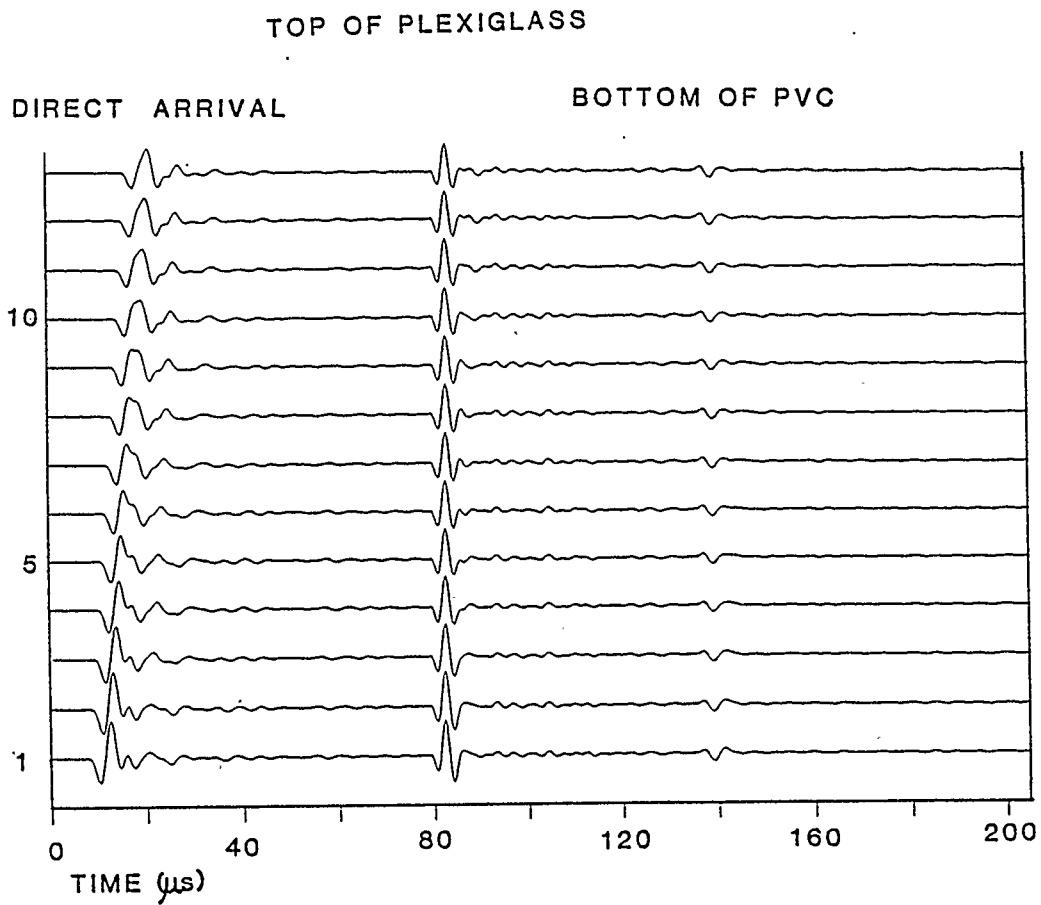


Figure 8-3: Sample of the Tank Data in Multics Format.

measurements then events on the synthetic traces match those on the tank data. Further details are provided below.

8.3 Wavelet Matching

The program computes ray amplitudes in the frequency domain, and in its original form, the amplitude spectrum of the zero-phase source wavelet was defined by a four-frequency trapezoid. This was modified so that a file containing the amplitude of each frequency component could be input instead. The direct arrival on the first trace of the tank data was sampled, and then Fourier transformed by means of a FFT algorithm (Press et al. 1986) into its frequency components (fig. 8-4). These frequency components were used to provide the input file for the source wavelet. Three separate peaks are visible in the spectrum of the input wavelet and these are probably related to the three square waves used to generate the source pulse. The program was then run using the parameters of the tank experiment, and a comparison was made between the resulting (synthetic) first reflection and the first reflection extracted from the tank data (fig. 8-5). Subtracting the tank wavelet from the synthetic resulted in some residual wavelet, which indicated some problem with the synthetic source wavelet. The actual source wavelet is somewhat

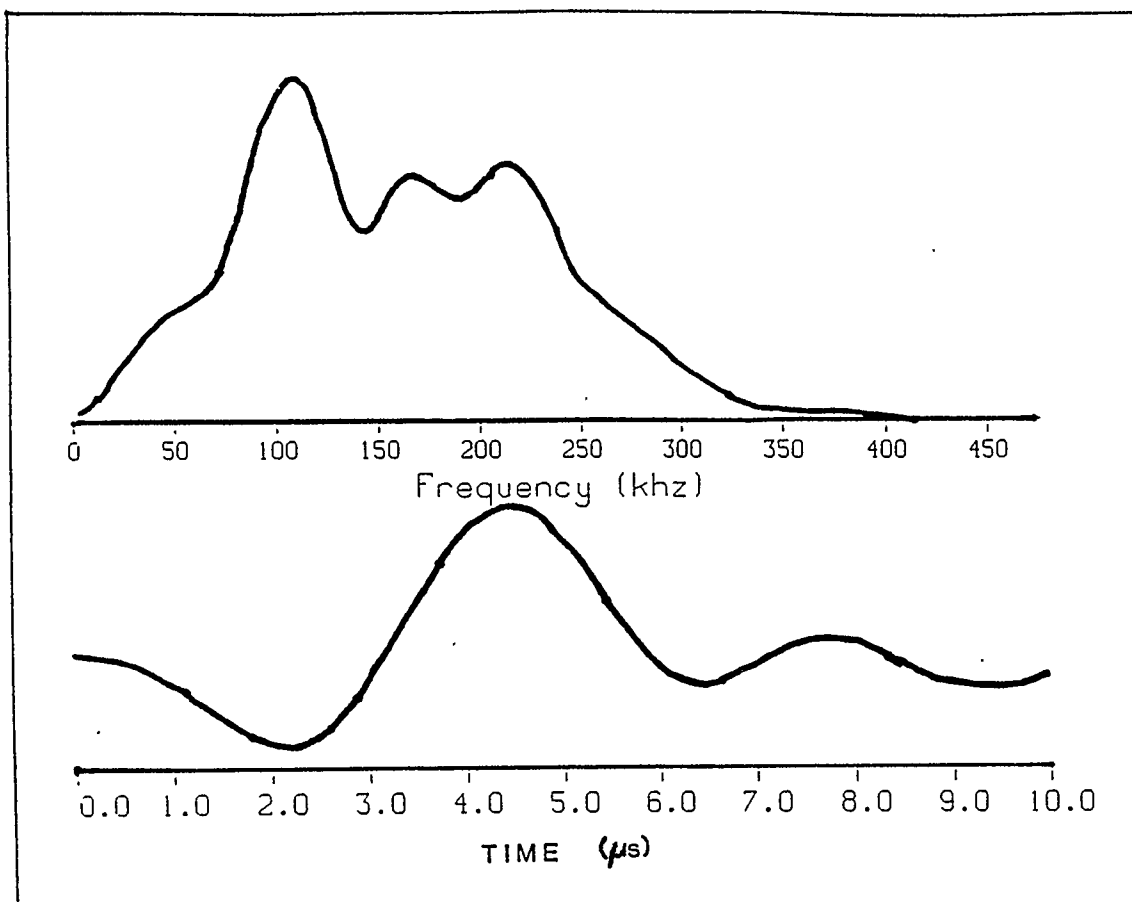


Figure 8-4: Extracted First Arrival and Spectrum (fig. 8-2, trace 1): The amplitude of each frequency was used to approximate the seismic tank source wavelet.

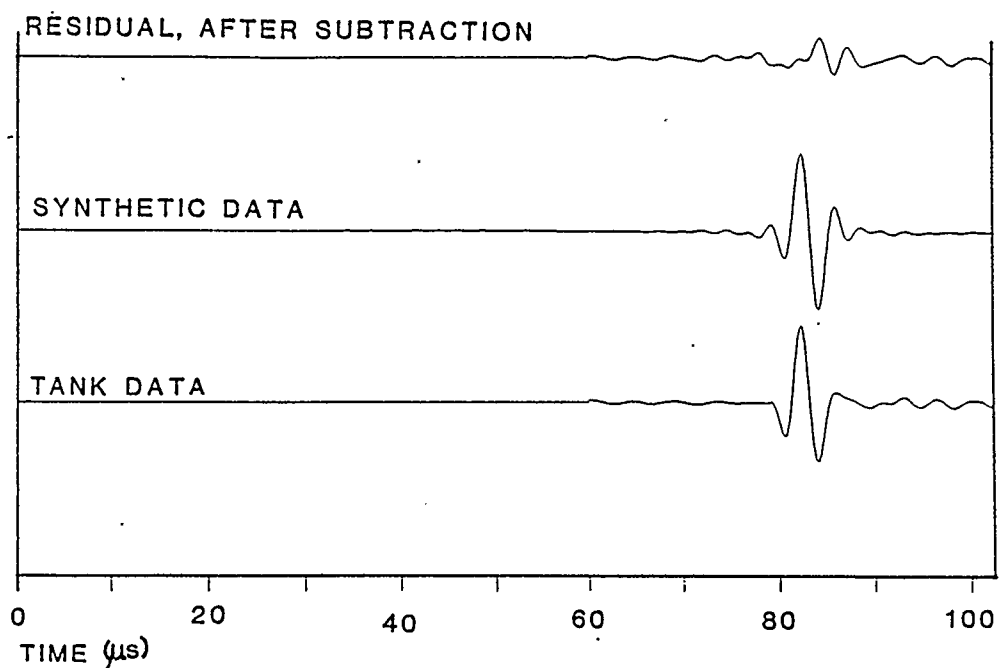


Figure 8-5: Comparison of the First Reflections from the Synthetic Data and the Tank Data: The synthetic trace is multiplied by a constant scale factor determined so that the peak amplitude equals that of the tank data. The residual is plotted at the same scale as the original wavelets.

'ringy' and so a perfect match to the synthetic data is unlikely. However, the source wavelet in the tank is not zero phase so the addition of a phase shift to the synthetic wavelet was investigated.

A series of synthetic traces were created using the same offset but rotating the source wavelet over a total of 90° . As can be seen in figure (8-6) this resulted in the first reflection being rotated from a minimum-phase to a zero-phase wavelet. Then the first event from the tank data (see fig. 8-5) was subtracted from each of the phase-rotated wavelets to give figure (8-7). The amount of residual appears to be minimized between traces 5 and 7, so the process was repeated to examine more closely the wavelets in this range (figures 8-8 and 8-9). Trace 6 on the subtraction plot (8-9) appears to be the minimum difference between the 'real' and synthetic data, although if trace 6 on figure (8-8) is compared with the data on figure (8-5), a front lobe is present which is absent from the tank wavelet. However, the match at this phase shift proved sufficiently close for the purposes of this investigation.

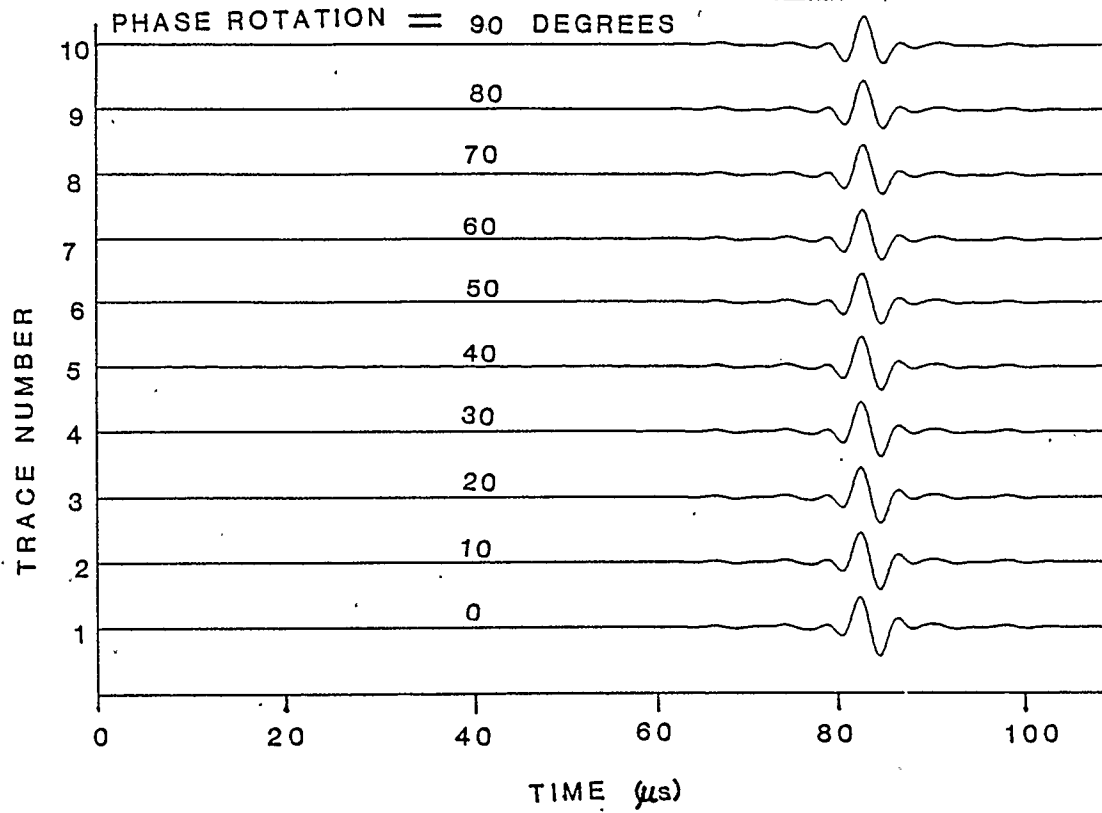


Figure 8-6: Phase Rotation Plot of the Synthetic First Reflection: All traces are at equal offset, with the source wavelet rotated by the indicated number of degrees.

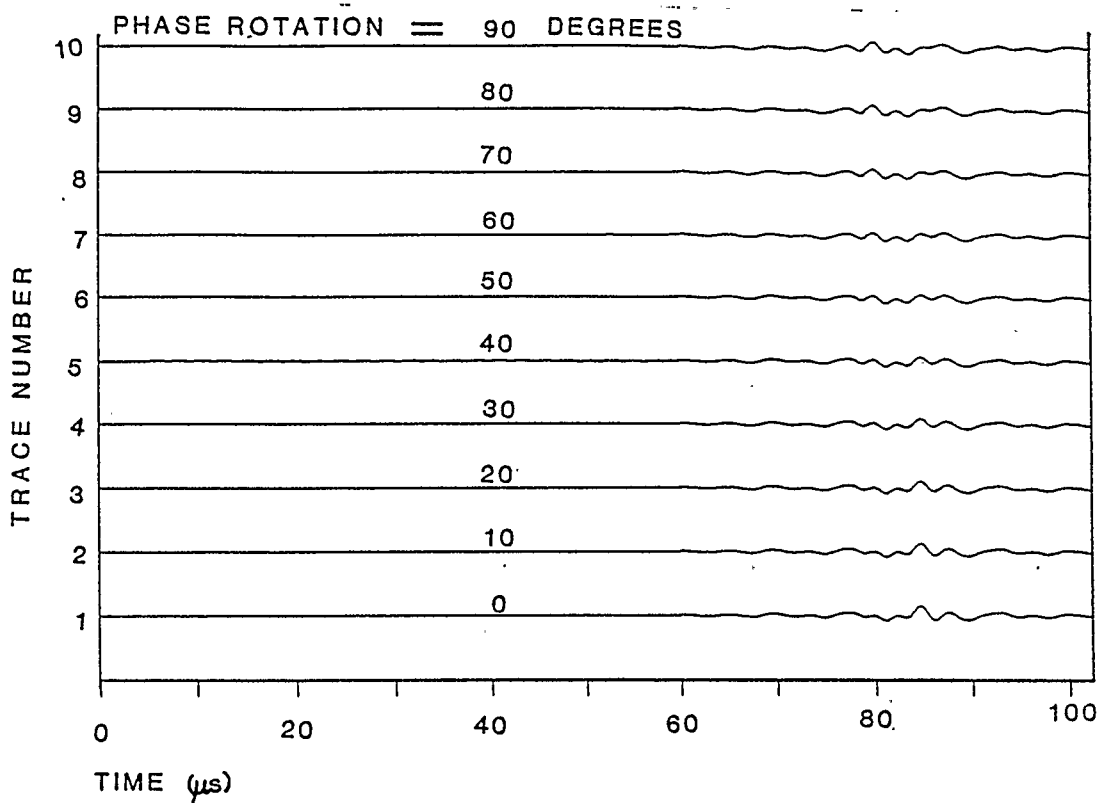


Figure 8-7: The Difference Between the Phase Rotated Synthetic Plot (fig. 8-6) and the Tank Data (fig. 8-5): The scaling is as in figure (8-5). The smaller the amount of residual, the closer the synthetic wavelet matches that used in the tank.

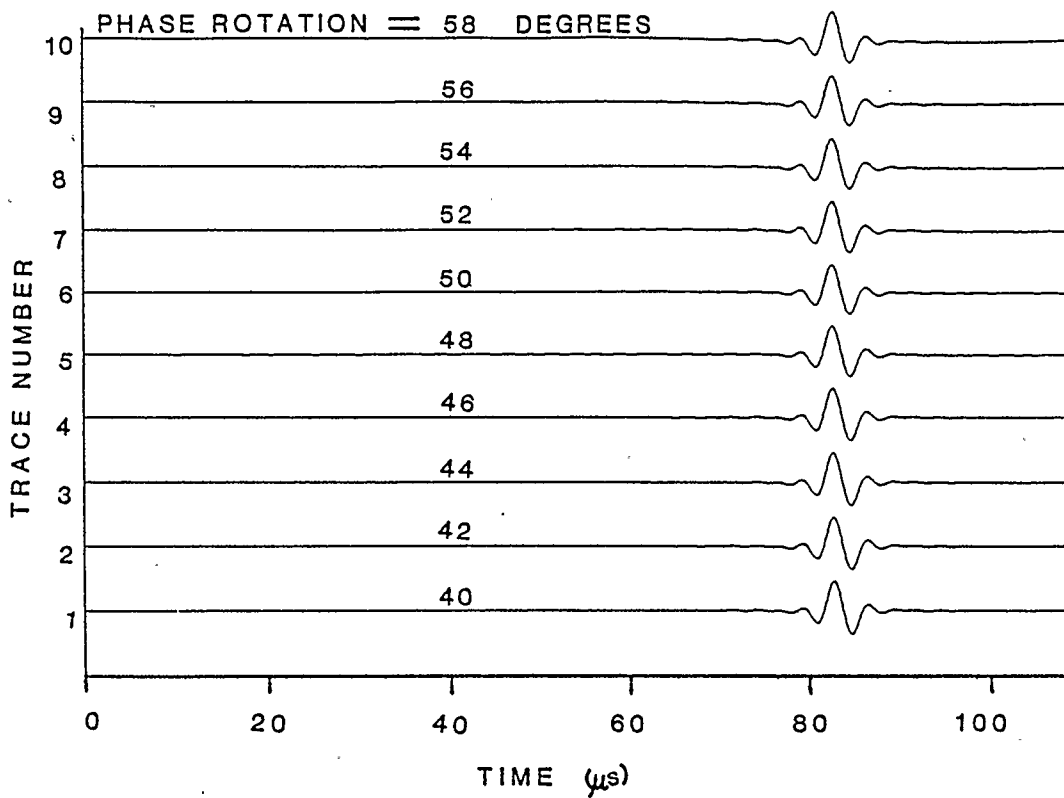


Figure 8-8: Refined Phase Rotation Plot of the Synthetic First Reflection: Similar to figure (8-6) but with a finer increment between phase rotations.

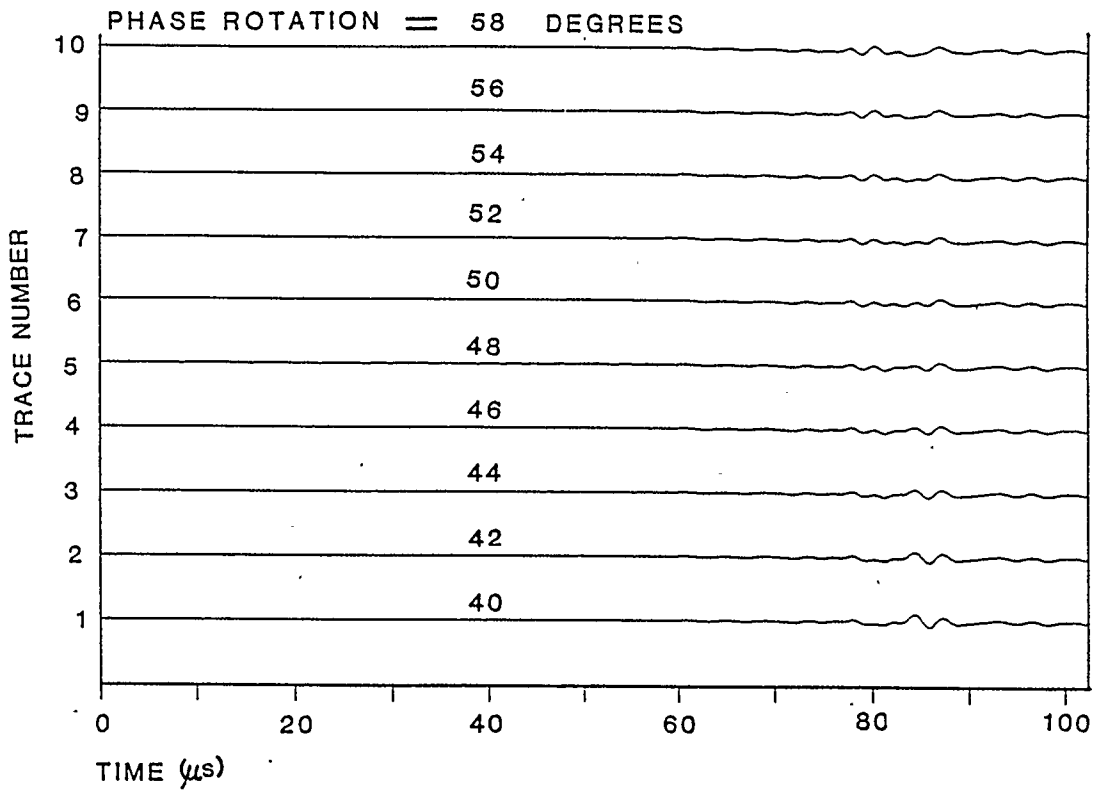


Figure 8-9: The Difference Between the Refined Phase-Rotated Synthetic Plot (fig. 8-8) and the Tank Data.

9. RESULTS AND DISCUSSION

9.1 Introduction

Once the survey parameters and source wavelet had been matched, direct comparisons were possible between the ray-tracing plots and those from the modelling tank. In this chapter comparisons are first made to ray tracing over anelastic models, and then to elastic models. Some comments about the critical angle are made and then the tank data are compared to plots of particle displacement. A discussion of the effects of the large receiver size concludes this chapter.

9.2 Anelastic Modelling

A comparison was made using the first 40 traces of the tank data, after removal of the direct arrivals (fig. 9-1). Complex ray tracing was done using the model parameters and the results are shown in figure (9-2). In order to detect any differences the tank data (fig. 9-1) were subtracted from the synthetic data (fig. 9-2), and the resulting difference plotted as figure (9-3). Since the first trace in figure (9-3) was used to determine the match of the source wavelet it shows a minimal amount of residual amplitude. There is a definite increase in residual

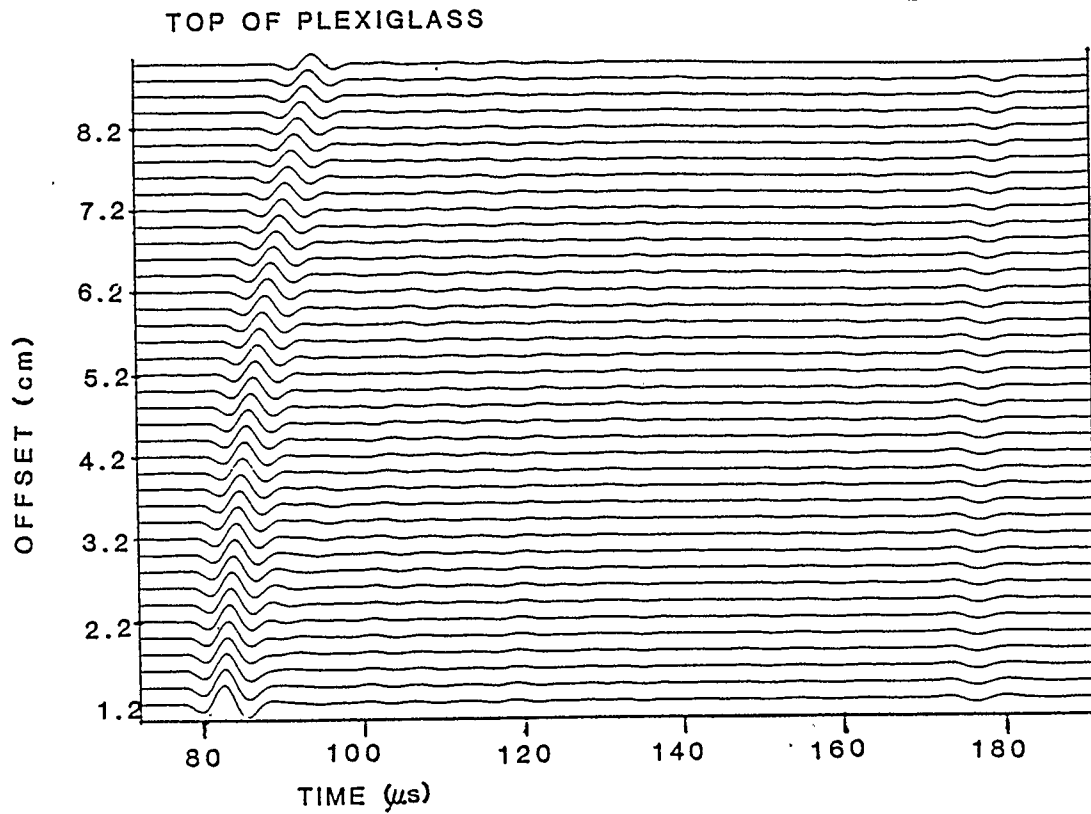


Figure 9-1: Tank Data With Direct Arrivals Removed: Traces are scaled by a constant scaling factor.

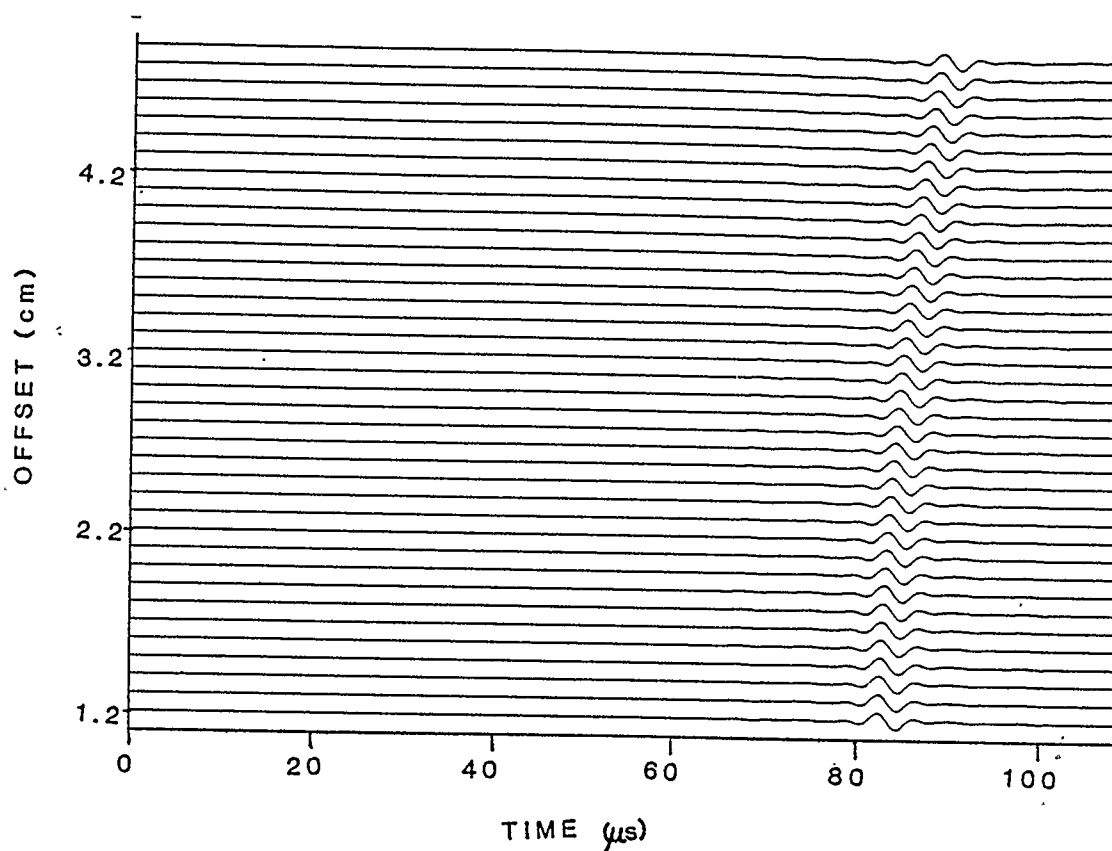


Figure 9-2: Synthetic Data Based on Tank Parameters, Including Attenuation: Parameters given in table 1, traces are scaled by a constant scaling factor.

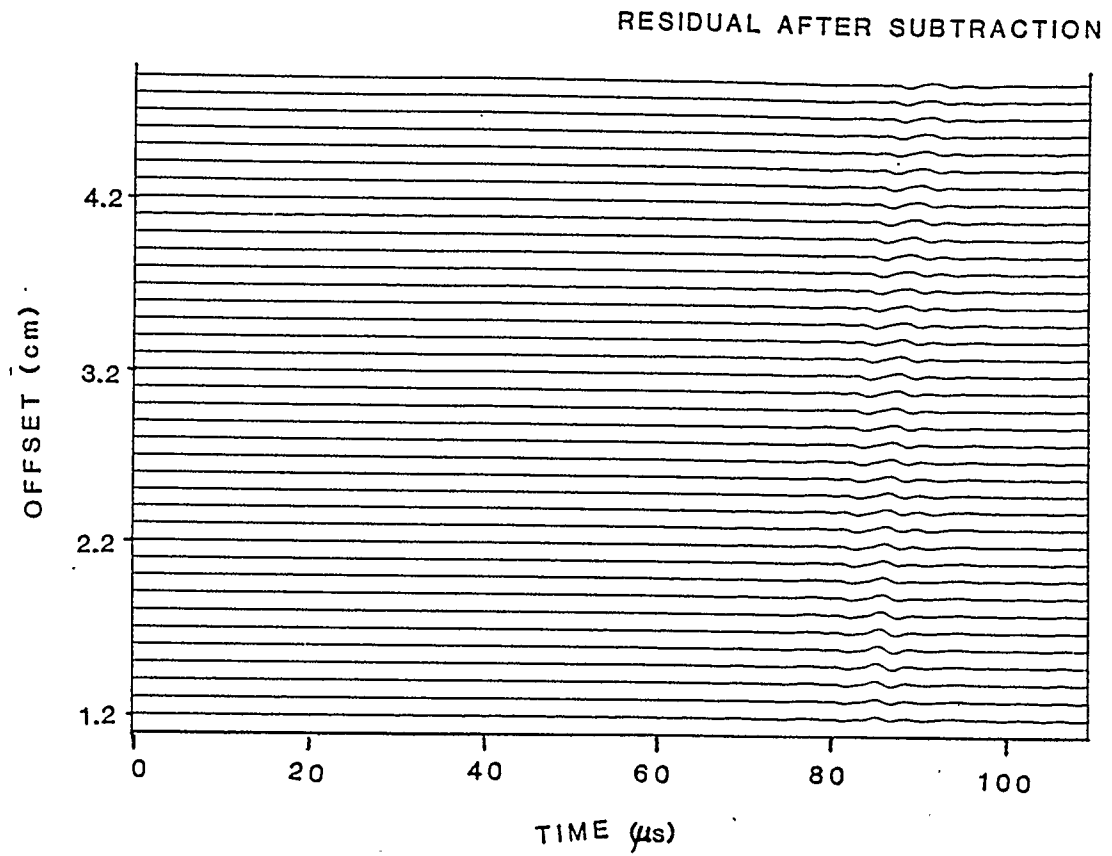


Figure 9-3: The Difference Between the Synthetic Data (fig. 9-2) and the Muted Tank Data (fig. 9-1).

amplitude over the next 5 or so traces but this levels off and remains fairly constant for the rest of the section. The residual wavelet appears to widen with increased offset which suggests that whatever its cause, the residual experiences attenuation of the higher frequencies with offset.

The difference between the tank data and the synthetic traces could be due to the following factors:

1. Imperfect matching of the source wavelet: To test this possibility the above subtraction process was repeated using the same source wavelet frequencies, but without the phase rotation (section 8.3). As can be seen in figure (9-4) if the source wavelet is not matched correctly the differences between the synthetic and tank data can increase with offset - although in this case the high-frequency content does not decrease with offset;

2. Incorrect matching of the model parameters: Since the first trace is not at zero offset, the time to the first reflection is affected by both the source-receiver offset and the distance between the transducers and the plexiglass. This problem is reduced by calculating the 'true' offset from the first breaks, and then calculating the depth to the first layer from the first reflection times. However, there is still some room for error, and in fact moveout curves show some discrepancy between the two data types (more below);

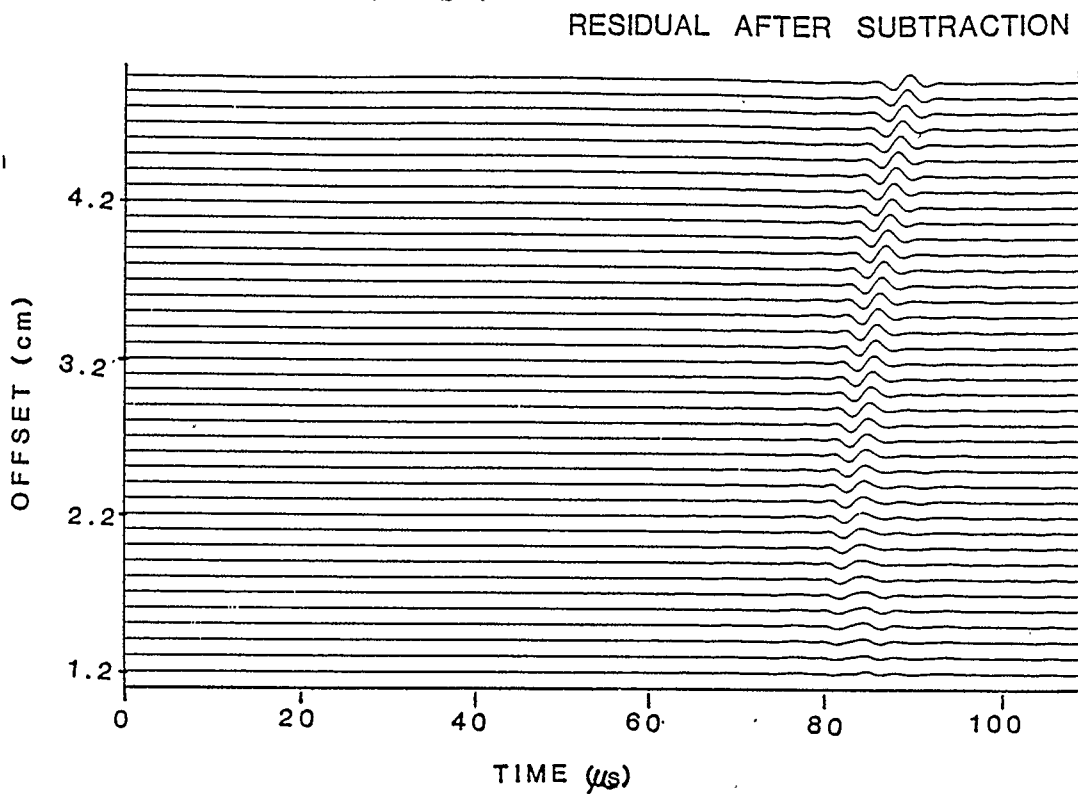


Figure 9-4: The Difference Between the Synthetic Data Without Phase Rotation of Source Wavelet and the Tank Data: Incorrect matching of the source wavelet results in a significantly larger amount of residual than when a phase rotated source wavelet is used.

3. Transducer effects: The response of the transducers may vary systematically according to the incident angle of an incoming wave, or they may contain 'hot' or 'cold' spots of varying amplitude response. As the exact mechanisms by which a transducer measures waves whose wavelengths are about a third of its own diameter are unknown, systematic changes in the response seem plausible;

4. Physical effects not accounted for by theory. Ray tracing is only an approximation of the full wavefield and is known to break down under certain conditions (e.g. at the critical angle, Červený and Ravindra 1971, p. 174). One of the goals of this work is to test the validity of complex ray tracing, and it would be presumptuous to assume that the cause of any discrepancies must lie elsewhere. However, effects from 3 would be difficult to separate from those due to 1 or 2, and it seems probable that some combination therein is the cause.

The data match proved sufficient for some investigations into changes of reflection amplitude due to changes in source-receiver offset. The amplitude of each reflection event, taken at its peak value, was calculated for both the synthetic traces and those of the tank data. To enable comparisons between the two data types, the synthetic amplitudes were multiplied by a constant scaling factor, determined to best fit tank data amplitude curves. The amplitudes were then plotted, as were the times (by

sample number) at which these amplitudes occurred (fig. 9-5). As can be seen in the upper part of figure (9-5) some discrepancies occur in the moveout of the two data sets, which lends some credibility to the argument that the experiment geometry has not been reproduced exactly. The amplitude curve of the synthetic trace fits within the variations of the tank data, with the exception of the first few traces. There appears to be a regular oscillation superimposed upon the tank data amplitudes. This effect is more pronounced on later plots and is discussed further below.

9.3 Comparison To Elastic Modelling

Elastic modelling was accomplished by repeating the ray tracing, using a Q value of infinity for the plexiglass sheet. Plots similar to figure (9-5) were created for the elastic case (fig. 9-6). The location of the critical angle is marked by a sharp amplitude rise on both sets of synthetic data. This effect is absent from the tank data, which can be explained by the fact that ray tracing breaks down at the critical angle (Červený and Ravindra 1971, p. 174), and the program does not include head waves. The amplitude plots are created by simply picking the largest positive amplitude on each trace. Beyond the critical angle we would expect to see a phase change and a decrease in

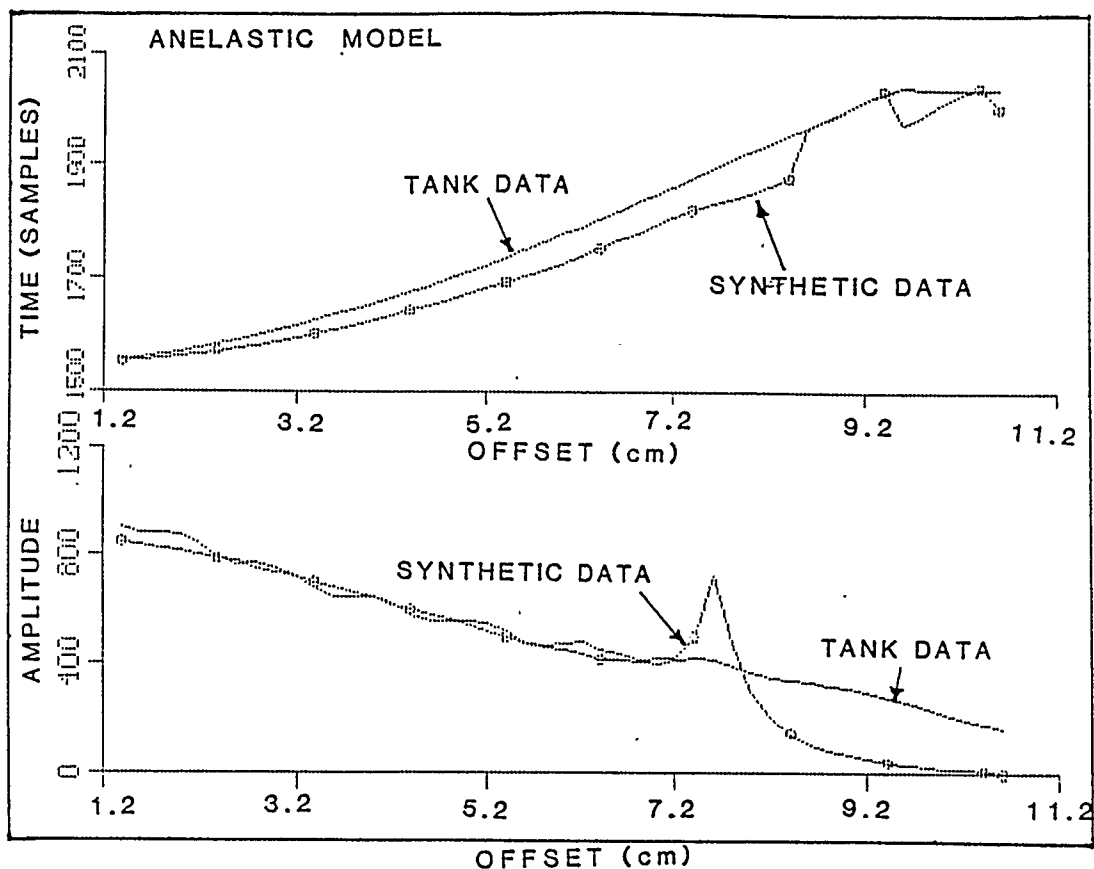


Figure 9-5: Anelastic Model Amplitude Curves Using the Full Offset Range: Amplitudes picked were the largest positive peak values, so that after the critical angle (indicated by the large peak in the synthetic data curve) it is the side lobe amplitudes which are picked. The synthetic data amplitudes were multiplied by a constant scaling factor picked so that the amplitudes on the tenth traces were equal.

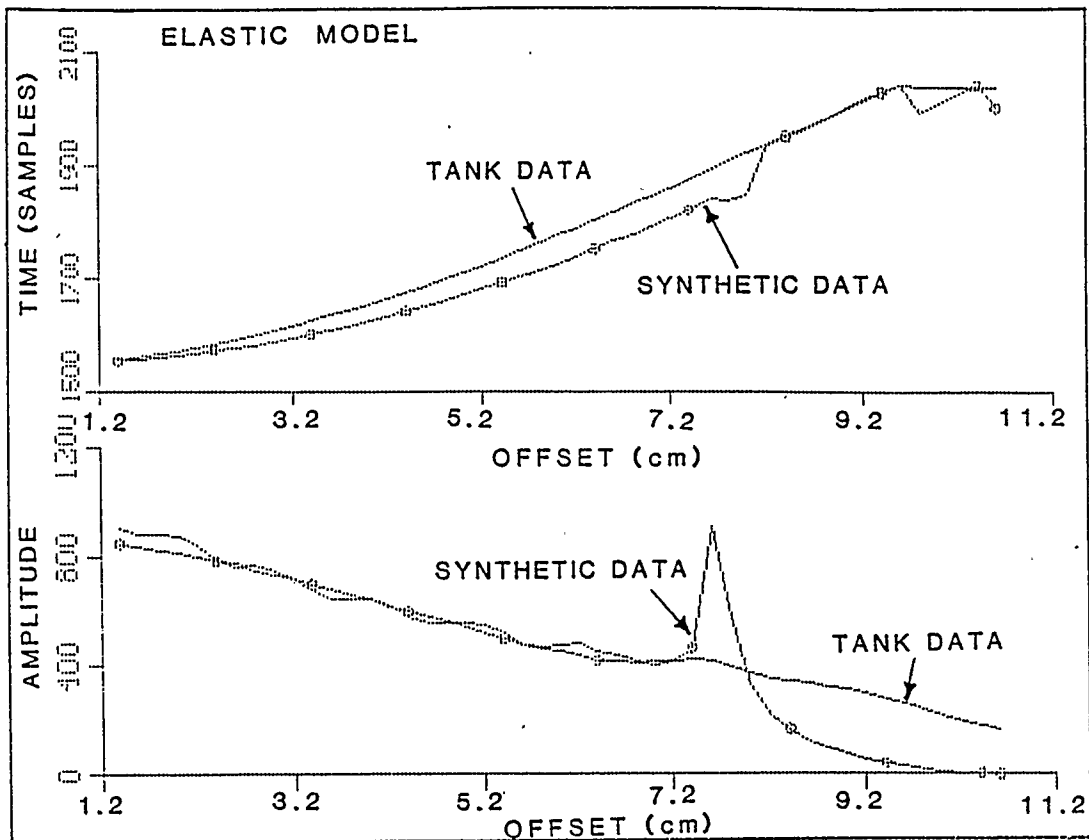


Figure 9-6: Elastic Model Amplitude Curves Using the Full Offset Range: Synthetic data does not include anelastic effects. The amplitudes are scaled in the same manner as figure (9-5).

amplitude similar to those which occur on the synthetic data. This suggests, that although no obvious change appears on the tank data, it is the head wave amplitude which is picked beyond the critical distance. The event on the tank data appears continuous, even though the head wave and reflection separate at the critical angle. This suggests that the reflection is masked by the head wave at this point.

Before the zone around the critical angle, the amplitude curves from the anelastic and elastic modelling match those of the tank data equally well (figures 9-5,6). At the critical angle both synthetic curves depart from the tank curve, although the anelastic curve is a somewhat better approximation. Beyond the critical angle comparisons are somewhat meaningless as ray theory does not take into account the existence of head waves.

The difference between the elastic and anelastic models was investigated by Fourier transforming the reflected wavelet on the last trace of each synthetic data set to obtain its amplitude spectrum (fig. 9-7,8). The spectrum from the anelastic model (fig. 9-7) and that of the elastic model (fig. 9-8) proved to be almost identical. For this model the only attenuation would occur at the reflecting interface (as the water was assumed to behave elastically), so the lack of spectrum change is not implausible. A greater difference would occur if the

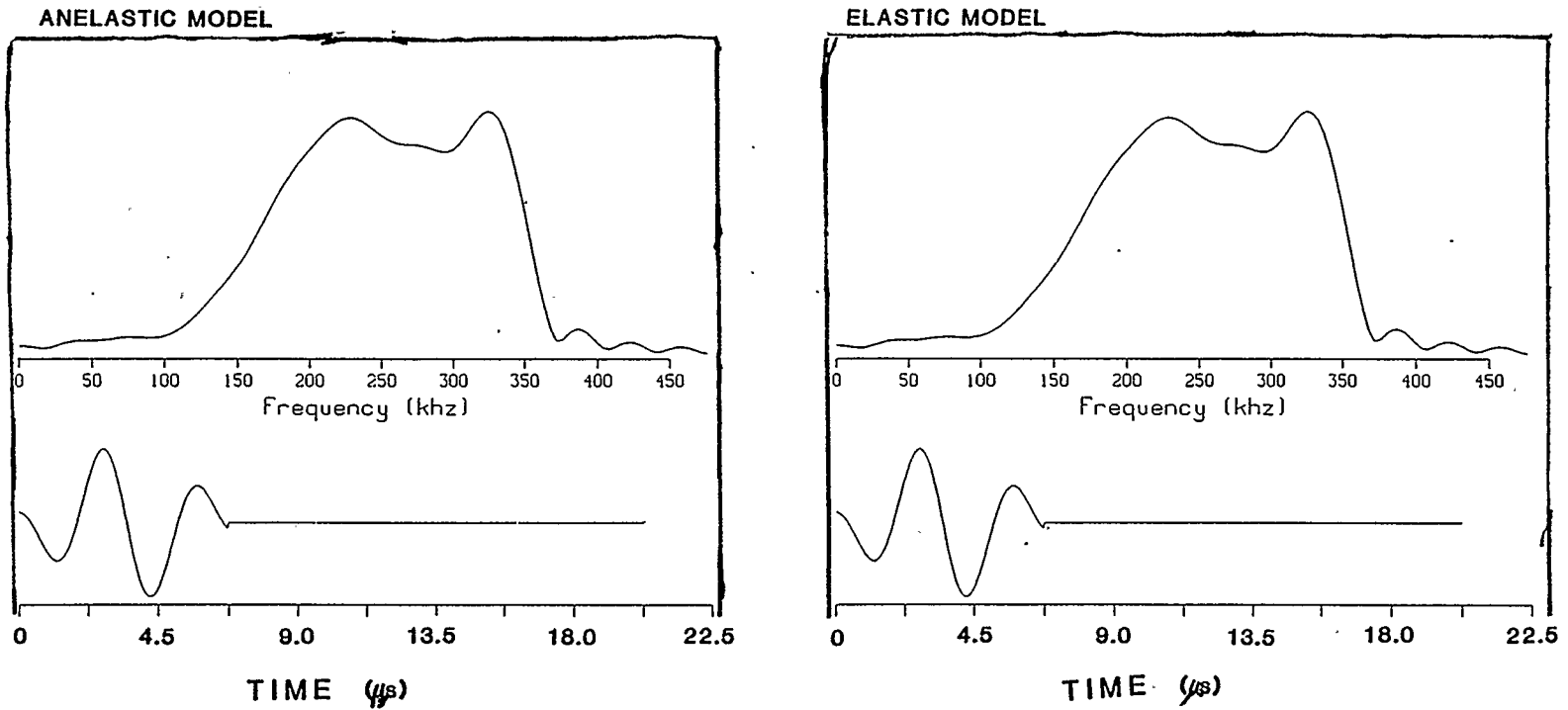


Figure 9-7: Synthetic Reflection Wavelet Including Anelastic Effects and Spectrum: Source-receiver offset = 5.0 cm.

Figure 9-8: Synthetic Reflection Wavelet Not Including Anelastic Effects and Spectrum: Source-receiver offset = 5.0 cm.

wavefield were to propagate through an anelastic medium, but it is the elastic/anelastic boundary that is investigated here.

9.4 Receiver Effects

The above comparisons were made by assuming that the piezoelectric transducer acts as a point receiver, and measures hydrostatic pressure. The second assumption was tested by modifying the original program to include the tank wavelet, and the reflection and transmission coefficients for the water layer. The result was a synthetic record that would have been produced had the receiver measured displacement instead of pressure (fig. 9-9). By subtracting the tank data from figure (9-9) (fig. 9-10), and comparing the amplitudes of these traces with those of the tank data (fig. 9-11) it becomes clear that it is not displacement which has been measured. This is an interesting observation when it is compared to the work of Dampney et al. (1972). They used a modelling system that consisted of piezoelectric transducers coupled directly to the surface of a plastic model. They suggested that

...the model experiences a displacement source which is detected by the acceleration (force) sensed by the receiver. By reciprocity in the model this functional relationship can be regarded as a force source being detected by a receiver sensitive to displacement.

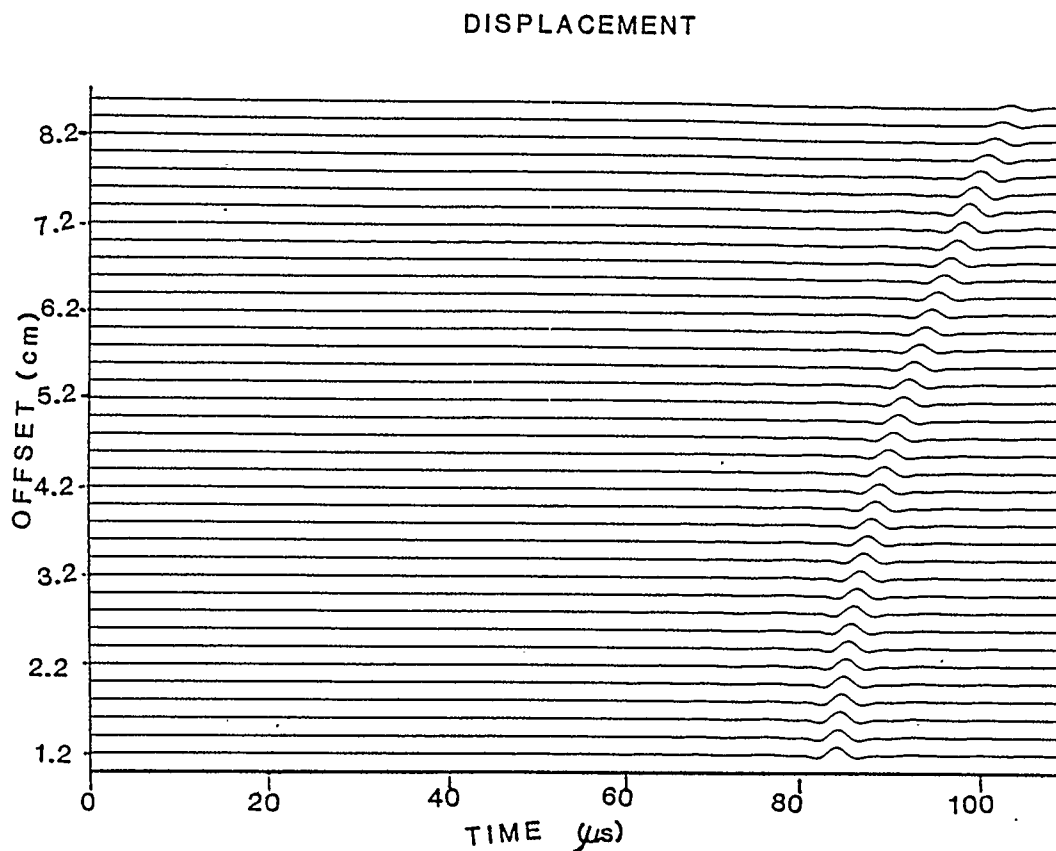


Figure 9-9: Synthetic Record Showing Particle Displacement Amplitudes: The original complex ray tracing program was modified to include the tank source wavelet, but not to convert the output to pressure amplitudes. The model parameters are given in Table 1., and include anelastic effects.

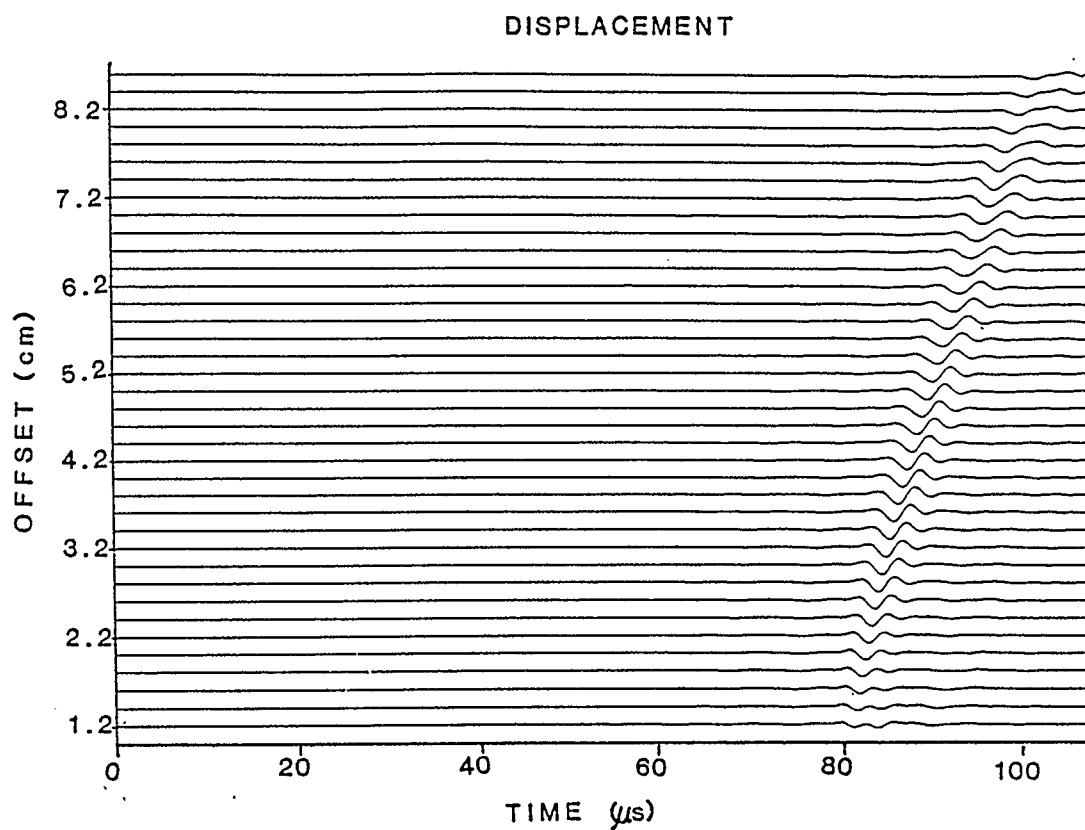


Figure 9-10: The Difference Between the Displacement Synthetic (fig. 9-9) and the Tank Data: The large amount of residual suggests that displacement amplitudes do not accurately model the tank data.

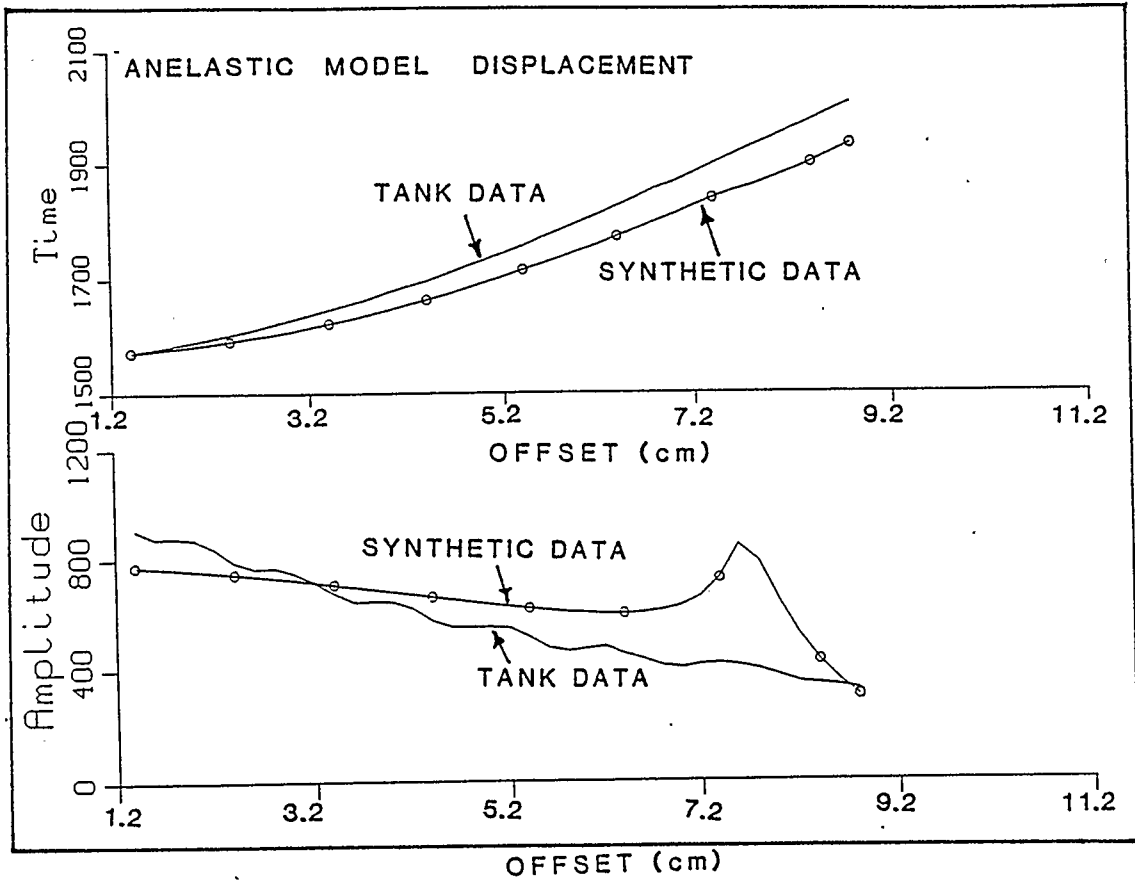


Figure 9-11: Particle Displacement Amplitude Curves Including Anelastic Effects: Synthetic data amplitudes are from figure (9-10), and are multiplied by a constant scaling factor such that the amplitudes from both data sets are equal at trace 10.

Dampney et al. (1972) used Lamb's problem to create synthetic seismograms, so the nature of the source was more relevant than when ray tracing is used. The coupling of the receivers to the medium is also different, however the basic processes involved are the same. For this reason it is important to keep the results of figure (9-11) in mind when discussing the basic assumptions inherent in physical modelling.

The fact that the source and receiver are too large to act as single points was taken into account by Dampney et al. (1972), who suggest that an average reading is taken over the contact area. This was not done in the present study. Although the amplitude curves for the complex ray tracing (which assumes a point-receiver) appear to match those from the tank data, some effects which may be due to the large receiver size are present. Before the critical angle is attained there is some wander in the amplitude curves of the tank data. This wander takes the form of a sine wave with a period of about 1.0 cm, which is slightly less than the radius of the transducers. This effect disappears after the critical angle, which may be due to the fact that the wave fronts change from curved for the reflection, to straight for the head wave. The physical reason for this is not clear but it is plausible that this may indeed be where certain assumptions break down. More work could be done on this problem, but the error involved

is small compared to the amplitude of the waves, and should not be a factor in most model experiments.

10. CONCLUSIONS AND FUTURE WORK

The validity of ray tracing in complex space was tested by comparing synthetic data traces generated with traces from a physical modelling experiment. This was accomplished using a ray-tracing program in which the output displacement amplitudes were converted to produce pressure amplitudes, similar to those measured by the physical modelling system. This conversion involved the derivation and implementation of a numerical differentiation algorithm which used variable station spacing and Lagrangian polynomials. With this program, the specific case of an elastic medium overlying an anelastic medium was used to investigate the initial value of the attenuation angle. The results of the above comparisons lead to the following conclusions:

1. Variable spacing Lagrangian differentiation is valid in complex space. The method converged even when station spacing varied over several orders of magnitude, despite the fact that stations with varying depth were artificially located in complex space.
2. Complex ray tracing is a valid method of reproducing reflection events generated by physical modelling experiments. Curves of change of amplitude with offset from

the ray-tracing program match similar curves from the tank data.

3. The change in amplitude with offset and the spectrum shapes are identical before the critical angle, whether or not anelastic effects are included in the ray-tracing model. There may be some instances when anelastic theory must be used, although in this experiment this is not the case.

4. The assumption that piezoelectric transducers, with diameters larger than the wavelengths they measure, act as point receivers sensitive to hydrostatic pressure appears to be valid.

5. Physical modelling using the seismic tank is sufficiently precise to enable competing mathematical theories to be compared. Amplitude curves were closely reproduced, although this experiment did not conclusively prove or disprove earlier work on the attenuation angle.

This leads to some suggestions for future work. The program could be expanded to include S waves, and then used to look for cases in which significant differences occur between elastic and anelastic modelling. Once these have been found, physical models that reproduce these conditions could be used to further test the validity of anelastic

theory. The program could also be expanded to include the amplitude of the direct arrivals so that comparisons of the absolute amplitudes of events would be possible. The addition of head waves would also be an asset, but this would require further theoretical development before implementation would be possible.

The combination of physical modelling with anelastic theory opens up many avenues of inquiry. One of the leading problems in exploration geophysics is the correlation of rock property laboratory measurements with those obtained from borehole measurements, and seismic surveys. The differences found are often attributed to dispersion of velocities due to attenuation. Materials in the tank can be tested directly and the results compared to seismic measurements, so that direct testing of theory becomes possible. As geophysics becomes an increasingly subtle science, these previously ignored effects in wave propagation may become deciding factors in the interpretation of seismic data for the delineation of subsurface geology.

REFERENCES

- Aki, K. and Richards, P.G.,(1980). Quantitative Seismology, Vols. 1 and 2, W.H. Freeman, San Francisco, CA, USA.
- Arfken, G.,(1985), Mathematical methods for physicists, Academic press inc.
- Bennett, J.A.,(1974), Complex rays for radio waves in an absorbing ionosphere, Proc. I.E.E.E.,62,1577-1585.
- Bertoni, H.L., Felsen, L.B. and Hessel, A.,(1971), Local properties of radiation in lossy media, I.E.E.E. Trans. Antennas Propagat.,AP-19,226-237.
- Bland, D.R.,(1960), The theory of linear viscoelasticity, Permagon, New York, NY.
- Borcherdt, R.D.,(1973), Energy and plane waves in linear viscoelastic media,J. Geophys. Res.,78,2442-2453.
- Borcherdt, R.D.,(1977), Reflection and refraction of type-II S waves in elastic and anelastic media, Bull. Seism. Soc. Am.,67,no.1,43-67.
- Borcherdt, R.D.,(1982), Reflection-refraction of general P- and type-I S-waves in elastic and anelastic solids, Geophys.J.R. astr. Soc.,70,621-638.
- Bourbiè, S. and Gonzalez-Serrano, A.,(1983), Synthetic seismograms in attenuating media, Geophysics,48,no. 12, 1575-1587.
- Buchen, P.W.,(1971), Plane waves in linear viscoelastic media, Geophys. J. R. astr. Soc.,23,531-542.
- Budden, F.R.S. and Terry, P.D.,(1971), Radio ray tracing in complex space, Proc. Roy. Soc. Lond.,25,97-113.
- Červený, V. and Ravindra, R.,(1971), Theory of seismic head waves, University of Toronto Press, Toronto.
- Cheadle, S.P., Bertram, M.B. and Lawton, D.C.,(1985), Development of a physical seismic modelling system, University of Calgary, Current Research, Part A, Geologic survey of Canada, paper 85-1A,499-504.
- Cheadle, S.P.,(1988), Seismic modeling of subsea permafrost, Ph.D. Thesis, Dept. of Geology and Geophysics, University of Calgary, Canada.

- Clay, C.S. and McNeil, H.,(1955), An amplitude study on a seismic model, Geophysics,20,766-773.
- Connor, K.A. and Felsen, L.B.,(1974), Complex space-time rays and their application to pulse propagation in lossy dispersive media, Proc. I.E.E.E.,62,1586-1598.
- Dampney, N.G., Mohanty, B.B. and West, G.F.,(1972) Calibrated model seismic system, Geophysics,37, no. 9,445-455.
- Evans, J.F., Hadley, C.F., Eisler, J.D. and Silverman, D., (1954), A three-dimensional seismic wave model with both electrical and visual observation of waves, Geophysics,19, 220-236.
- Felsen, L.B.,(1984), Geometrical theory of diffraction, evanescent waves, complex rays and Gaussian beams, Geophys.J. R. astr. Soc.,79,77-88.
- Grove, W.E.,(1966), Brief numerical methods, Prentice-Hall, inc. Englewood Cliffs, N.J.
- Hall, S.H.,(1956), Scale model seismic experiments, Geoph. Prosp.,4,348-364.
- Hearn, D.J. and Krebs, E.S.,(1988), Complex rays applied to wave propagation in a viscoelastic medium, Pre-print.
- Jordan, N.F.,(1966), Attenuation and dispersion of shear waves in plexiglass, Geophysics,31,621-624.
- Kelly, L.G.,(1967), Handbook of numerical methods and applications, Addison-Wesley Pub., Reading, Massachusetts.
- Krebs, E.S.,(1983a.) Discrepancies in energy calculations for inhomogeneous waves, Geophys. J. R. astr. Soc.,75,839-846.
- Krebs, E.S.,(1983b.) The viscoelastic reflection/transmission problem: Two special cases, Bull. Seism. Soc. Am.,73,no. 6,1673-1683.
- Krebs, E.S. and Hearn, D.J.,(1985), On the geometrical spreading of viscoelastic waves, Bull. Seism. Soc. Am., 75, no. 2,391-396.
- Krebs, E.S. and Hron, F.,(1980a.), Ray-synthetic seismograms for SH waves in anelastic media, Bull. Seism. Soc. Am.,70, no. 1,29-46.

- Krebes, E.S. and Hron, F., (1980b.), Synthetic seismograms for SH waves in a layered anelastic medium by asymptotic ray theory, Bull. Seism. Soc. Am., 70, no. 6, 2005-2020.
- Levin, F.K. and Hibbard, H.C., (1955), Three-dimensional seismic model studies, Geophysics, 20, 19-32.
- McDonald, J.A., Gardner, G.H.F. and Hilterman, F.J., ed. (1983), Seismic studies in physical modeling, IHRDC Publ., Boston, Mas.
- Oliver, J., Press, F. and Ewing, M., (1954), Two-dimensional model seismology, Geophysics, 19, 202-219.
- Press, F., Oliver J. and Ewing, M., (1954), Seismic model study of refractions from a layer of finite thickness, Geophysics, 19, 388-401.
- Press, W.H., Flannery, B.P., Teukolsky, S.A. and Vetterling, W.T., (1986), Numerical recipes: The art of scientific computing, Cambridge University Press, Cambridge England.
- Sheriff, R.E. and Geldart, L.P., (1982), Exploration seismology Volume 1: History, theory, and data acquisition, Cambridge University Press, Cambridge.
- Silva, W., (1976), Body waves in a layered anelastic solid, Bull. Seism. Soc. Am., 66, no. 5, 1539-1554.
- Silverman, D., (1969), Mapping the Earth with elastic wave holography, IEEE Trans. Geoscience. Electron., GE-7, 190-199.
- Slawinski, M.A., (1988), Inhomogeneous elastic body waves, M.Sc.Thesis, Dept. of Geology and Geophysics, University of Calgary, Canada.
- Terada, T. and Tsuboi, C., (1927), Experimental studies on elastic waves (part I), Bull. Earth. Res. Inst., Tokyo Imperial Univ., 3, 55-63.
- Toksöz, M.N. and Johnston, D.H., ed. (1981), Seismic wave attenuation, Geophysics reprint series No. 2, S.E.G. press. Tulsa, Oklahoma.
- Wuenschel, P.C., (1965), Dispersive waves - an experimental study, Geophysics, 30, 539-546.